Quaternary Science Reviews 269 (2021) 107130

Contents lists available at ScienceDirect

Quaternary Science Reviews

journal homepage: www.elsevier.com/locate/quascirev

Lacustrine leaf wax hydrogen isotopes indicate strong regional climate feedbacks in Beringia since the last ice age

W.C. Daniels [a, b, *], J.M. Russell [a], C. Morrill [c, d], W.M. Longo [a], A.E. Giblin [b], P. Holland-Stergar [a], J.M. Welker [e, f], X. Wen [g], A. Hu [h], Y. Huang [a]

[a] Department of Earth, Environment and Planetary Science, Brown University, 324 Brook St., Providence, RI, 02912, USA
[b] The Ecosystem Center, Marine Biological Laboratory, 7 MBL St., Woods Hole, MA, 02543, USA
[c] Cooperative Institute for Research in Environmental Sciences, University of Colorado, Boulder, CO, 80309, USA
[d] National Centers for Environmental Information, NOAA, 325 Broadway, Code E/NE33, Boulder, CO, 80305, USA
[e] Department of Biological Sciences, University of Alaska, Anchorage, Anchorage, AK, USA
[f] Ecology and Genetics Research Unit, University of Oulu, Finland & UArctic, Finland
[g] Department of Atmospheric and Oceanic Sciences, Peking University, Beijing 100871, China
[h] Climate and Global Dynamics Laboratory, National Center for Atmospheric Research, Boulder, CO, 80305, USA

ARTICLE INFO

Article history:
Received 1 March 2021
Received in revised form
28 July 2021
Accepted 29 July 2021
Available online 21 August 2021

Handling Editor: Yan Zhao

Keywords:
Holocene
Last glacial maximum
Paleoclimatology
Arctic Alaska
Continental biomarkers
Leaf wax hydrogen isotopes

ABSTRACT

The Late-Quaternary climate of Beringia remains unresolved despite the region's role in modulating glacial-interglacial climate and as the likely conduit for human dispersal into the Americas. Here, we investigate Beringian temperature change using an ~32,000-year lacustrine record of leaf wax hydrogen isotope ratios (δ^2H_{wax}) from Arctic Alaska. Based on Monte Carlo iterations accounting for multiple sources of uncertainty, the reconstructed summertime temperatures were ~3 °C colder (range: −8 to +3 °C) during the Last Glacial Maximum (LGM; 21-25 ka) than the pre-industrial era (PI; 2–0.1 ka). This ice-age summer cooling is substantially smaller than in other parts of the Arctic, reflecting altered atmospheric circulation and increased continentality which weakened glacial cooling in the region. Deglacial warming was punctuated by abrupt events that are largely synchronous with events seen in Greenland ice cores that originate in the North Atlantic but which are also controlled locally, such as by the opening of the Bering Strait between 13.4 and 11 ka. Our reconstruction, together with climate modeling experiments, indicates that Beringia responds more strongly to North Atlantic freshwater forcing under modern-day, open-Bering Strait conditions than under glacial conditions. Furthermore, a 2 °C increase (Monte Carlo range: −1 to +5 °C) over the anthropogenic era reverses a 6 °C decline (Monte Carlo range: −10 to 0 °C) through the Holocene, indicating that recent warming in Arctic Alaska has not surpassed peak Holocene summer warmth.

1. Introduction

During the last glacial termination, the Arctic experienced some of the most extreme temperature changes known in recent geologic time. In the North Atlantic region, this includes up to 23 °C of warming from 25 ka to present (Dahl-Jensen et al., 1998) and abrupt changes on the order of 4–14 °C such as the Bølling-Allerød (BA), and the Younger Dryas (YD) (Johnsen et al., 1992; Grootes et al., 1993; Severinghaus and Brook, 1999; Buizert et al., 2014). The magnitude and rate of these changes are linked to changes in the strength of the Atlantic meridional overturning circulation (AMOC) and feedbacks from sea ice (Broecker et al., 1989; Li et al., 2005) that cause temperature changes to be larger than anywhere else on earth – a phenomenon known as "Arctic Amplification" (Shakun and Carlson, 2010). Based on paleoclimate records, Miller et al. (2010) estimate that Arctic temperature change exceeds that of the northern hemisphere by a factor of 3–4. This finding, however, is weighted heavily by the estimate of Last Glacial Maximum (LGM) cooling which has high uncertainty as it is derived primarily from the Greenland ice core borehole temperatures (Dahl-Jensen et al., 1998; Miller et al., 2010) which may not represent temperature changes over the entire Arctic (Shakun and

* Corresponding author. Department of Earth, Environment and Planetary Science; Brown University; 324 Brook St., Providence, RI, 02912, USA.
E-mail address: wcdaniels@geo.umass.edu (W.C. Daniels).

https://doi.org/10.1016/j.quascirev.2021.107130
0277-3791/

Carlson, 2010). Additional continuous paleotemperature records extending through the LGM are needed to better understand the spatiotemporal variations in Arctic Amplification, and its underlying physics.

Eastern Beringia, the region today encompassing Alaska and the Yukon Territory, also experienced dramatic environmental changes during the last glacial-interglacial transition. Several paleoenvironmental archives extend through the last glacial period, owing to the lack of regional glaciation during the LGM. Major changes included the submergence of the Bering Land Bridge, the expansion of peat soils (Jones and Yu, 2010) as well as trees and shrubs (Eisner and Colinvaux, 1992; Oswald et al., 1999; Mann et al., 2010), retreat of mountain glaciers (Hamilton, 2003; Pendleton et al., 2015), permafrost degradation (Mann et al., 2010), the loss of megafauna (Mann et al., 2013), and the appearance of humans (Goebel et al., 2008). Questions remain, however, about the temperature changes during the deglacial period. Some Arctic Alaskan pollen-based estimates suggest LGM temperatures were actually warmer than present (Bartlein et al., 2011). Lower sea levels increased the continentality of Alaska and may have weakened summertime cooling (Mann et al., 2001; Bartlein et al., 2015). Climate models further predict that Laurentide Ice Sheet (LIS) orography steered warm air into Alaska during the LGM maintaining relatively mild or even warmer temperatures relative to the present (Broccoli and Manabe, 1987; Otto-Bliesner et al., 2006; Bartlein et al., 2011; Tierney et al., 2020). However, pollen-based temperature reconstructions are limited because Pleistocene ecosystems of Beringia have no modern analog, while different climate models predict different, and often opposite, temperature changes in Arctic Alaska in response to changes in LIS height (Fig. S1), calling this mechanism into question.

Within the last glacial termination, much of the Arctic experienced abrupt climate events associated with Heinrich Stadial 1 (HS1), the BA, and the YD. In Eastern Beringia, evidence for BA-YD climate reversals is found in both marine (Praetorius and Mix, 2014) and terrestrial records (Engstrom et al., 1990; Epstein, 1995; Mann et al., 2002; Meyer et al., 2010; Young et al., 2019), although several locations show no YD signal (Kurek et al., 2009b). The magnitude of temperature changes during these abrupt transitions is not tightly constrained in Alaska, but is thought to be weaker than in the North Atlantic (Hu et al., 2006; Graf and Bigelow, 2011). In addition to these millennial-scale events, resubmergence of the Bering land bridge and establishment of Bering Strait throughflow between 13.4 ka and 11.0 ka (Keigwin et al., 2006; England and Furze, 2008; Jakobsson et al., 2017; Pico et al., 2020) likely had considerable influence on local Beringia climate. Sites adjacent to the Bering Strait cooled in summer and warmed in winter in response to an increasingly maritime climate (Mann et al., 2001; Bartlein et al., 2015), although the spatial ramifications of this transition are unconstrained. This effect may have been partially offset by the initiation of north-flowing ocean currents and heat transport from the North Pacific into the Western Arctic, warming broader Beringia (Hu et al., 2012), a hypothesis which requires more investigation. Bering Strait status is also proposed to modulate the North Pacific circulation response to deglacial freshwater release events in the North Atlantic (Hu et al., 2012). For example, during HS1 (~15-18 ka), collapse of AMOC is associated with an invigoration of Pacific Meridional Oceanic Circulation (PMOC) (Okazaki et al., 2010; Maier et al., 2018), minimizing or even reversing temperature changes in the North Pacific relative to the North Atlantic (Sarnthein et al., 2006). Warm sea surface temperatures during HS1 may have influenced continental Beringia, as suggested by chironomid-inferred warming from 17–14 ka at Zagoskin Lake in Alaska (Kurek et al., 2009a), although more records are needed to confirm this.

Here, we generate a centennially-resolved record of temperature change from the northern foothills of the Brooks Range mountains (68.643 °N, 149.458 °W, Fig. 1) to examine the amplitude and causes of temperature changes from Arctic Alaska during the LGM, the last deglaciation, and the Holocene. This new dataset, alongside paleoclimate data-model comparisons, provide new insight into the large-scale and regional controls on temperature change in this part of the Arctic.

2. Materials and methods

2.1. Lake setting and core chronology

Lake E5, located in Alaska's North Slope (Fig. 1), is a glacial lake containing sediments extending through the LGM (Eisner and Colinvaux, 1992), providing an extraordinary opportunity to examine deglacial climate change in the Western Arctic. Meteorological observations at the nearby Toolik Field Station, approximately 5 km to the west, show that mean annual temperature averages −8.5 °C, summer temperatures (JJA) average 9 °C, and precipitation averages 312 mm with 60% falling during summer (Cherry et al., 2014).

The study lake is situated on glacial deposits dating to 780–125 ka (Hamilton, 2003). It is 12 m deep and typically ice-free from early June to mid-September. Gravity cores were retrieved from a boat in 2011 and 2012, and in May 2014, overlapping sediment cores were recovered using a Bolivia and modified Livingstone square-rod piston corer through the ice from the deepest point in the lake. Core images and magnetic susceptibility (MS) profiles were generated with a GeoTek multisensor core logger (MSCL).

The previously-published chronology for the Lake E5 composite core (Fig. 2) is based on ^{210}Pb (Table S1) and 16 radiocarbon dates (Table S2) (Vachula et al., 2019; Longo et al., 2020). ^{210}Pb was measured on core Tool12-E5-1 B using gamma spectroscopy (Appleby et al., 1986). Ages and age uncertainty were modeled using the constant rate of supply (Appleby and Oldfield, 1978; Binford, 1990), and these data were incorporated into the composite core age model as non-radiocarbon age constraints.

The materials analyzed for radiocarbon consist of both plant and aquatic insect fragments (Table S2), both of which may be prone to over-estimating depositional ages in Arctic lakes. Terrestrial components can incur pre-aging on the landscape prior to transport into the lake (Abbott and Stafford, 1996). To address this, Oswald et al. (2005) suggested that small, non-woody plant fragments are least prone to landscape pre-aging and provide the most reliable depositional ages. In the Lake E5 cores, the plant-derived radiocarbon dates come from ultrasmall fragments of grasses and moss. Recently developed spectrometry techniques for ultrasmall samples (Shah Walter et al., 2015) were used for the analyses.

Where terrestrial plant fragments were absent, aquatic organisms were measured for radiocarbon. Aquatic insect remains can overestimate sediment deposition ages in Arctic lakes due to incorporation of ^{14}C-depleted methane, DOC, or DIC into aquatic food webs (Abbott and Stafford, 1996; Wooller et al., 2012). We tested for this effect by independently dating insect eggs and plant fragments from the 24.5–25.5 cm horizon, and insect eggs and daphnia ephippia from the 113.5–115.5 cm horizon (Table S2). No significant age differences are observed between organic materials. This, together with recent findings that radiocarbon ages of lake-derived methane from Northern Alaska is surprisingly young (Elder et al., 2018), indicate that incorporation of pre-aged carbon into aquatic organisms is minimal and justifies the use of aquatic macrofossils in the age model.

Ages were modeled using the Clam version 2.2 (Blaauw, 2010) with IntCal13 (Reimer et al., 2013). The Clam settings were:

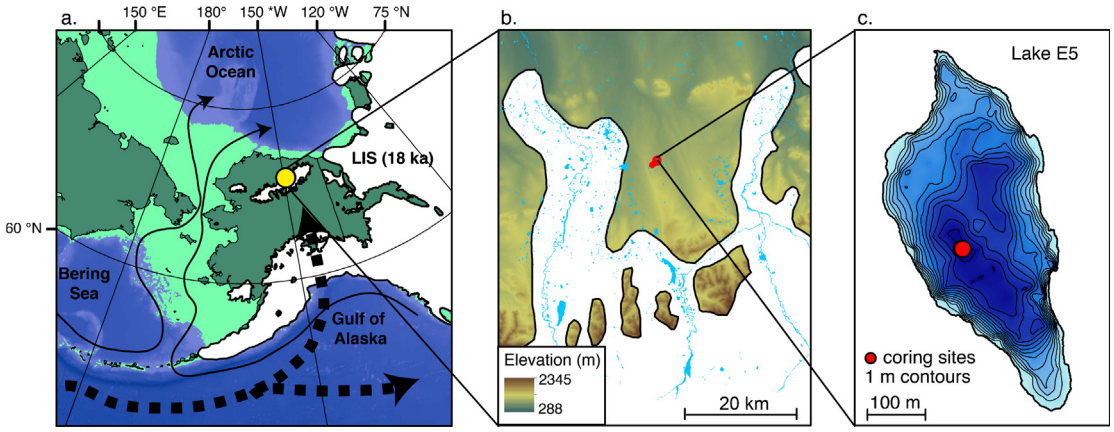

Fig. 1. a) Map of Beringia with ice extent 18,000 calendar years before present (18 ka) (Dyke, 2004) and E5 study lake (yellow dot). Dark and light green show modern and approximate LGM coastline, respectively. Bold dashed arrows represent the LIS-orography forced northward advection of subpolar air into Alaska as simulated in CCSM3 (Otto-Bliesner et al., 2006). Solid arrows are modern surface currents through the Bering Strait (Stabeno et al., 1999). b) study area showing surface waters, the Lake E5 watershed (red), and the maximum glacier extent of the late-Wisconsin glaciation (Manley and Kaufman, 2002). c) Lake E5 bathymetry Toolik GIS, 2019) and coring sites. (For interpretation of the references to colour in this figure legend, the reader is referred to the Web version of this article.)

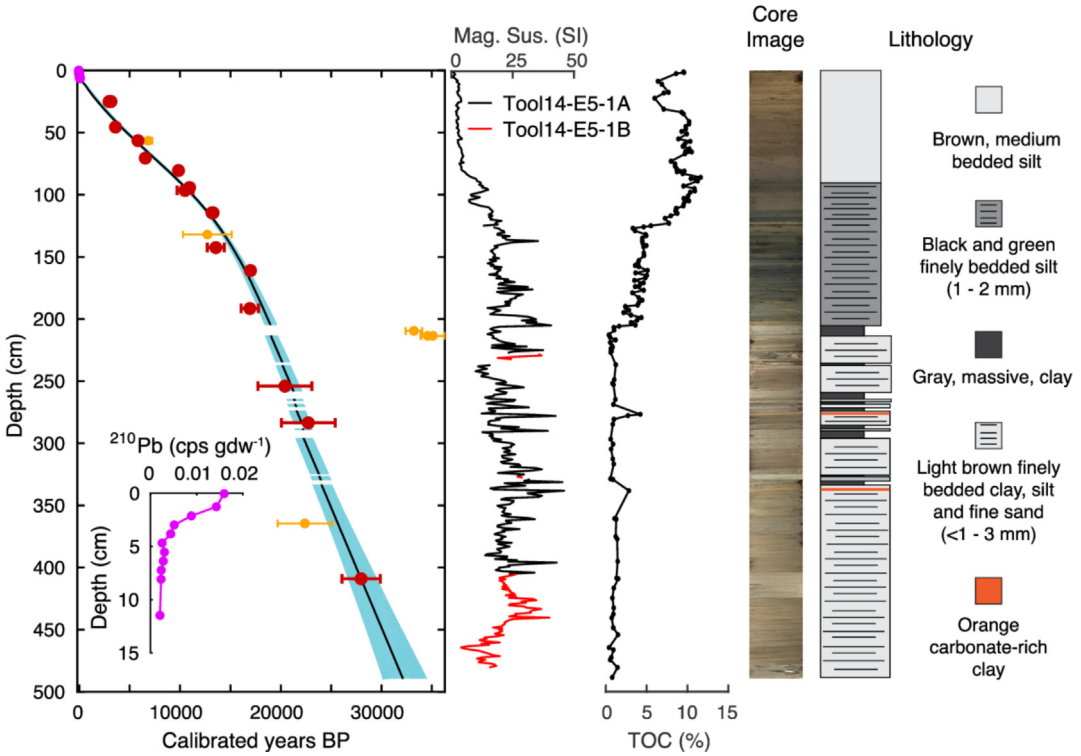

Fig. 2. Age model and lithologic profiles for the Lake E5 sediment core. Radiocarbon ages are calibrated using the Intcal13 calibration curve (Reimer et al., 2013). The spline and 95% error envelope were modeled in clam.R software (Blaauw, 2010). Orange points are outliers and not included in the CLAM model. The magenta inset curve shows ^{210}Pb concentration measured using gamma spectroscopy. Instantaneous deposition events are shown as gaps. (For interpretation of the references to colour in this figure legend, the reader is referred to the Web version of this article.)

type = 4, wgts = 1, smooth = 0.6. A series of discrete sedimentary beds are modeled as slump events in the Clam software, and leaf wax isotope measurements were omitted from these intervals.

2.2. Leaf wax hydrogen isotope analysis

Hydrogen isotope ratios of terrestrial leaf waxes (C_{28} *n*-acid; hereafter δ^2H_{wax}) were measured in Lake E5 sediments as a proxy for changes in past $\delta^2H_{precipitation}$ and climate. Lipids were extracted from 1 to 5 g of dry sediment using a Dionex accelerated solvent extractor with 9:1 dichloromethane:methanol. Total lipid extracts were separated using aminopropyl silica gel chromatography with 2:1 dichloromethane:isopropanol and 4% acetic acid in ether as eluents. Acid fractions were spiked with an internal standard of *cis*-eicosenoic acid, then methylated overnight at 60 °C in acidified methanol of known isotopic composition. Further purification of fatty acid methyl esters (FAMEs) was performed with silica gel chromatography with dichloromethane and hexane as eluents. The concentration of FAMEs were determined using gas chromatography with a flame ionization detector.

Hydrogen isotope ratios of FAMEs were analyzed on a Thermo Finnegan Delta XL GC-IRMS at Brown University. Each sample was injected at least twice, targeting the *n*-C_{28} acid to be in the range of 3–5 V. The δ^2H values are reported relative to VSMOW in delta notation, and analytical uncertainties are reported in Table S3 δ^2H_{wax} values are mathematically corrected for the methyl groups added during derivatization.

2.3. Temperature estimation

Previous quantitative reconstructions of $\delta^2H_{precipitation}$ from measurements of δ^2H_{wax} have demonstrated the need to account for glacial-interglacial changes in oceanic $^2H/^1H$ ratios (Konecky et al., 2016). We correct for this effect across the last glacial termination by subtracting the δ^2H_{ocean} anomaly from the measurements of δD_{wax}. The δ^2H_{ocean} anomaly is determined by assuming LGM ocean was 1‰ enriched in $\delta^{18}O$ relative to today (Schrag et al., 1996), scaling the 1‰ glacial-interglacial change to the foramanifera-inferred changes in $\delta^{18}O$ (Lisiecki and Raymo, 2005), then converting to δ^2H by multiplying by 8.

Additionally, determination of $\delta^2H_{precipitation}$ from δ^2H_{wax} is improved by accounting for changes in terrestrial plant assemblages (Feakins, 2013; Konecky et al., 2016), as the $^2H/^1H$ fractionation between water and lipids (ε_{app}) varies among plant types (Sachse et al., 2012; Gao et al., 2014). At Lake E5, the Holocene is characterized by greater abundance of dicot shrubs, particularly of the genera *Betula, Salix,* and *Alnus*, whereas during the LGM, grasses (*Poaceae*) were relatively abundant (Livingstone, 1955; Eisner and Colinvaux, 1992; Abbott et al., 2010). During the glacial termination, transient peaks in *Artemesia* and sedges of the *Cyperaceae* family are evident around 16 and 11-15 ka, respectively (Eisner and Colinvaux, 1992; Abbott et al., 2010).

Despite the recognition of variable ε_{app} among Arctic plants (Wilkie et al., 2012; Daniels et al., 2017; Daniels et al., 2018; Berke et al., 2019; Dion-Kirschner et al., 2020; O'Connor et al., 2020), there are few δ^2H_{wax} studies which attempt to correct for vegetation changes in the Arctic (Nichols et al., 2014). $^2H/^1H$ fractionation estimates are not available for all Arctic taxa, so here we follow methods of Feakins (2013) and Nichols et al. (2014) by broadly grouping plant taxa, and applying an end-member mixing model to estimate past ε_{app} values (Fig. S3). The broad plant groupings include monocot and dicot plants, as in Nichols et al. (2014), and the ε_{app} end-members are scaled to the fraction of monocot and dicot represented in the previously documented pollen spectra from Lake E5 (previously called "Oil Lake"; Eisner and Colinvaux, 1992) which was depth-correlated to our stratigraphy based on organic carbon profiles and a distinct marker bed dating to the beginning of the deglaciation. Generally, monocotyledonous plants fractionate more strongly than dicotyledonous plants (Gao et al., 2014).

Several estimates of ε_{app} are available from the Arctic for specific plants taxa and for integrated sediments (Wilkie et al., 2012; Daniels et al., 2017; Berke et al., 2019; McFarlin et al., 2019). We opt to use local landscape-scale ε_{app} values determined from a 24-lake surface sediment training set in the Alaskan tundra which includes Lake E5 (Daniels et al., 2017). More negative ε_{app} values for C_{28} *n*-acids are associated with a predominance of wet sedge tundra or grasses while lakes within dicot-dominated forb/shrub tundra exhibit weaker fractionation. Based on a regression between C_{28} ε_{app} and landcover type, we select endmember ε_{app} values of −135‰ (1σ = 20‰) to represent monocot taxa and −96‰ (1σ = 16‰) for dicot taxa. These end member choices are comparable to fractionation values for modern plants. The ε_{app} of arctic shrubs, including *Betula nana*, *Salix* sp., and others, ranges from −96‰ to −108‰ (Daniels et al., 2017; Dion-Kirschner et al., 2020; O'Connor et al., 2020). Fractionation factors of graminoids are more variable − C_{28} *n*-acid of *Eriophorum vaginatum* (monocot sedge) in Alaska exhibits ε_{app} of −159‰ (Daniels et al., 2017), whereas *Carex* sp. analyzed in Greenland had ε_{app} of just −98‰ (Dion-Kirschner et al., 2020). Nichols et al. (2014) used endmember of −114‰ and −159‰, somewhat more negative than our choices but with a comparable amount of spread between them, such that the correction would be similar in a relative sense. Inclusion of species-level endmembers or broader geographic calibration may improve the mixing model, although the differentiation between monocots and dicots clearly elucidated by Gao et al. (2014) and Sachse et al. (2012) should provide a first-order correction for changing plant assemblages.

There are several assumptions inherent in the quantitative conversion from δ^2H_{wax} to $\delta^2H_{precipitation}$. First, we assume that the C_{28} *n*-acids are derived from land plants (Chikaraishi and Naraoka, 2007) and are geochemically stable in sediments (Yang and Huang, 2003). While long chain (>C_{24}) *n*-acids can also be produced by aquatic vegetation, terrestrial tundra plants produce considerably higher concentrations of *n*-alkanes and *n*-acids than submerged and emergent aquatic vegetation of tundra lakes (Dion-Kirschner et al., 2020). Furthermore, our observations during repeated sampling of the lake by the Toolik Long-Term Ecological Research suggest that macrophytes are not particularly abundant and the littoral zone is characterized by cobbles and soft sediment. The low light penetration and extremely oligotrophic status of Lake E5 (Daniels et al., 2015) suggests that terrestrial sources dominate the long chain waxes.

Additionally, vegetation corrections are likely imperfect because of uncertainty in the pollen-wax production ratios among different plants. For example, pollen assemblage has little predictive capacity on leaf wax δ^2H in the tropical Pacific island lakes (Ladd et al., 2021); an assessment relating pollen directly to leaf wax signatures is needed for the Arctic. Furthermore, pollen assemblages from Arctic lakes may record regional signals and exhibit lags in response to climate change (Crump et al., 2019), and the methods here assume that the leaf waxes and pollen both respond similarly and rapidly to climate change. Nonetheless, a pollen-based approach has been used previously with success (Feakins, 2013), despite introducing a high degree of quantitative uncertainty (Dion-Kirschner et al., 2020).

To estimate temperature from $\delta^2H_{precipitation}$, we use the temperature-$\delta^2H_{precipitation}$ relationship determined from 20 years of precipitation monitoring at the Toolik Field Station (Klein et al., 2015), approximately 5 km west of and at a similar elevation to Lake E5. Over the 20 years of monitoring, precipitation sampling for $^{18}O/^{16}O$ and $^2H/^1H$ was opportunistic, included all seasons, including winter, made possible by researchers and field staff on site 12 months per year. Specific precipitation events were neither targeted nor avoided. Average daily temperatures during days when precipitation was collected were extracted from the Toolik Environmental Data Center (Toolik Environmental Data Center Team, 2016). We tested the δ^2H-temperature relationship further using an isotope-enabled version of the Community Atmosphere Model (IsoCAM) to examine changes in the slope of the $\delta^2H_{precipitation}$-T relationship at 1000-year time slices over the past 20 kyr in Alaska, as the relationship between these variables might be expected to change with major moisture source changes (Tharammal et al., 2013; Liu et al., 2014; Thomas et al., 2014). Monthly temperatures were extracted from each time slice for 40 years from 6 grid cells that cover Northern Alaska, and we analyzed the relationship between temperature and $\delta^2H_{precipitation}$ on these data.

All vegetation corrections and temperature conversions were performed in a Monte Carlo simulation in order to propagate uncertainty estimates of the δ^2H_{wax} measurements (average 1σ = 1.3‰, Table S3), the pollen-inferred vegetation assemblages

(ie. fraction monocot and fraction dicot; 1σ prescribed at 0.05), $^{2}H/^{1}H$ fractionation endmember values (uncertainty reported above), and the temperature-$\delta^{2}H_{precipitation}$ relationship and associated uncertainty reported below. Monte Carlo simulations were performed using 1000 iterations. To assess temperature changes between discrete time slices, we performed two-tailed Student's t-tests on the Monte Carlo distributions after compositing results for each time point within the periods of interest.

2.4. Climate model simulations

We use the Community Climate System Model 3 (CCSM3) global circulation model to test the effect of Bering Strait opening/closure and other glacial/interglacial boundary conditions on Beringian temperature and on Beringian sensitivity to global freshwater forcing events. The model has fully coupled atmosphere, land, ocean, and sea ice sub-models with a horizontal resolution of T42 or 2.8° for atmospheric and land models and nominal 1° with enhanced meridional resolution to 1/3° in the equatorial tropics for the ocean and sea ice models. Boundary conditions are provided by Hu et al. (2015) and include changes to the Laurentide Ice Sheet, orbital forcing, and atmospheric greenhouse gas concentrations. Surface temperatures were averaged over 100 years under 15 ka boundary conditions with an open and closed Bering Strait, and under present-day (1990 A.D.) boundary conditions with an open and closed Bering Strait. The model scenarios are idealized and not meant to represent the exact conditions under which the Bering Strait was flooded. Additionally, the same model configurations are used to test the effect of freshwater addition to the North Atlantic on Beringian climate. Under the four scenarios described above (15 ka open/closed, 0 ka open/close), freshwater was gradually added to the North Atlantic until the AMOC collapsed, at which point surface temperatures from Beringia for the succeeding 100 years were averaged.

3. Results

3.1. Modern precipitation isotopes

A total of 254 precipitation events at the Toolik Field Station were collected and analyzed, documenting a significant relationship between air temperature and $\delta^{2}H$ (Fig. 3). From this same dataset, Klein et al. (2015) use the $\delta^{18}O$-temperature regression, $\delta^{18}O = 0.354\ T - 21.11$, to reconstruct temperatures at the McCall glacier over the past 70 years. For $\delta^{2}H$, the total least squares regression has a slope of 0.292‰ °C^{-1}, equivalent to 3.4 °C ‰$^{-1}$. This value is in close agreement with the slope observed in other parts of Arctic North America (Porter et al., 2016). The root mean square error of the calibration is quite high at 7.9 °C, similar to the RMSE based on the $\delta^{18}O$, which is 7.2 °C.

3.2. Core chronology and lithology

Figure S2 shows the composite profile of overlapping core sections tied with distinct marker beds. The total core recovery was 500 cm, although there is significant distortion of bedding plains in the basal sections and so we only consider 480 cm of core in the composite here (Fig. 2). The lowest radiocarbon sample dates to 28,488 ± 1001 (1σ) calendar years before present, and extrapolation of the lower sedimentation rate produces a basal date of 32,086 ± 2197 (2σ) cal. yr BP. The 95% confidence interval ranges from ±4 years at the core top to ±2208 years at the base, and averages ±810 years throughout the entire record. The age model is less-tightly constrained within the last glacial period.

Glacial-interglacial changes are evident in the magnetic susceptibility (MS), total organic carbon (TOC), and lithology profiles (Fig. 2), and give rise to 3 distinct units that broadly correspond to the LGM, the last deglacial period, and the Holocene. The lower part of the core is characterized by low TOC (Vachula et al., 2019), averaging 4.9%, and magnetic susceptibility ranging from 0.5 to 46. A transition zone is apparent from 205 to 103 cm, wherein TOC increases from less than 1% to 8-12%, and MS decreases. Above this transition zone physical properties are more stable, although TOC generally decreases upwards. Sediments consist of laminated, light brown, clay-to fine sand-sized material in the lower sections, laminated, black, silt from 205 to 103 cm, and massive, brown, silt from 103 cm to the coretop.

There is a series of sedimentary beds comprised of distinct gray clay (205-213 cm, 235-237 cm, 258.5—264 cm, 266-268 cm, 271—273.5 cm, 285-288 cm, 289.5—295.5 cm, 325-326 cm, 330-332 cm, 332.5—333 cm). Based on the sharp contact boundary with underlying sediments, these clay beds are interpreted as instantaneous depositional events. Sediment cores from Lake NE14, approximately 10 km from Lake E5, reveal a series of similar sedimentary units characterized by high clay content and a distinct geochemical signature (Chipman et al., 2016). The occurrence of these units in NE14 is linked to shoreline thermo-erosion events during exceptionally warm or wet summers. In Lake E5, radiocarbon ages of macrofossils from two of these layers are approximately 35,000 ^{14}C yr bp (Fig. 2), suggesting they contain aged terrestrial fragments and are likewise derived from periglacial erosion events along the shoreline.

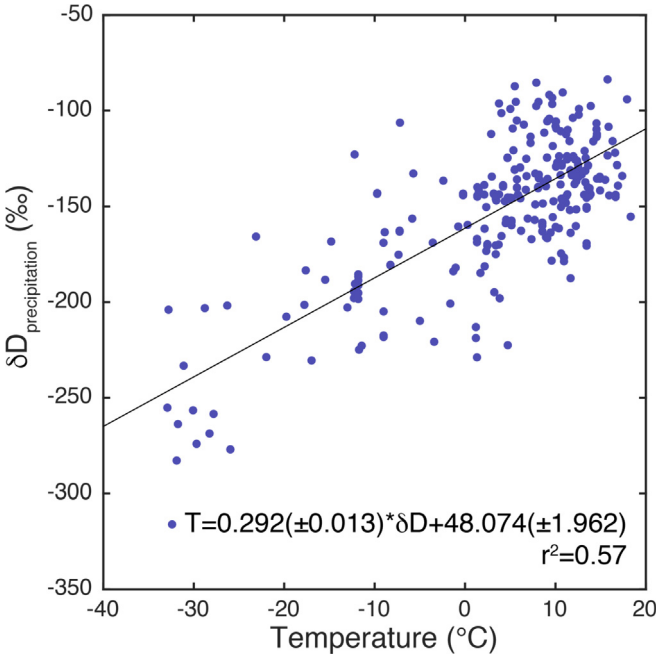

Fig. 3. Modern relationship between $\delta^{2}H_{precipitation}$ and air temperature at Toolik Lake, AK based on 254 precipitation events, supported in part by USNIP (US Network for Isotopes in Precipitation (Welker, 2000; Welker, 2012).

3.3. n-Acid distributions, $^{2}H/^{1}H$ ratios, and vegetation correction

Leaf wax *n*-acids are present throughout the Lake E5 core, with the sum of *n*-C_{16}-C_{32} ranging from an average of 59 μg g sed^{-1} in the glacial-aged sediments to 1596 μg g sed^{-1} in the Holocene sediments (Fig. 4). The carbon preference index is fairly high, averaging 5.8 ± 2.2, indicating that the waxes are derived from "fresh" plants and have undergone relatively little degradation (Bray and Evans,

1961) – they are unlikely to be sourced from shales in the Brooks Range mountains. The average chain length averages 25.3 ± 0.8, and is highest in the deglacial sediments (Fig. 4). Higher average chain length values are associated with greater aridity in the Arctic (Andersson et al., 2011), although Keisling et al. (2017) suggest that ACL also varies in response to temperature and vegetation change at Lake El'gygytgyn in Arctic Russia. Recent assessments from arctic tundra document that there is no clear relationship between plant taxa and *n*-acid homologue distributions (Dion-Kirschner et al., 2020; O'Connor et al., 2020). Thus it remains difficult to elucidate what drove the change in *n*-acid ACL. We note the increased ACL corresponds to higher representation of graminoid taxa in the pollen spectra, and suggest that ACL change reflects the plant community turnover during the deglacial period.

The raw δ^2H_{wax} values of C_{28} and C_{26} *n*-acids from Lake E5 are highly correlated ($r^2 = 0.74$, Fig. S4), indicating that these compounds share common terrestrial sources. We focus on the C_{28} δ^2H_{wax}. Values range from −280‰ to −244‰ and the record exhibits distinct glacial-interglacial structure characterized by more negative values during the last glacial period, a peak in the early Holocene, and a declining trend thereafter until the last 150 years (Fig. 5). The most pronounced change is a step-increase in δ^2H_{wax} centered at 11.6 ± 0.2 ka, coinciding with the termination of the Younger Dryas stadial. Other Alaska isotope records that span the YD interval, namely $\delta^{18}O$ of ice wedges (Meyer et al., 2010) and $\delta^{18}O$ of willow stems (Epstein, 1995; Gaglioti et al., 2017) also show a rapid increase at the termination of the YD (Fig. 6). In these records, pre-YD $\delta^{18}O$ values are comparable to the post-YD values, suggesting the YD was a brief interruption between Bølling and early Holocene warmth as is evident in Greenland ice core $\delta^{18}O$ (Buizert et al., 2014). In contrast, δ^2H_{wax} values of the Bølling warm period do not achieve post-YD values at Lake E5 and are only slightly ^2H-enriched relative to LGM samples. One possibility for this contrast is if the water isotope proxies record different seasons and the Bølling-Allerød temperature change was more pronounced in winter than summer as it was in the North Atlantic region (Atkinson et al., 1987; Denton et al., 2005). Given that the willow stems analyzed by Gaglioti et al. (2017) are thought to capture the same seasonality as the leaf waxes, however, it is more likely that a temporary expansion of graminoid sedges during the Bølling-Allerød and late deglacial (Eisner and Colinvaux, 1992; Abbott et al., 2010) impacted the record of δ^2H_{wax}, masking a potential BA signal. A slight shift toward longer carbon chain lengths in the *n*-acid distributions in the deglacial sediments is evidence for a potential vegetation effect on the leaf waxes. Because Arctic graminoids express stronger $^2H/^1H$ fractionation than dicotyledenous shrubs or forbs (Daniels et al., 2017, 2018; Berke et al., 2019), the observed vegetation change would suppress a change in δ^2H_{wax} during the Bølling interval.

The effect of the vegetation-based correction (Fig. S3) is most notable during the deglacial period, and brings the Bølling-to post-YD differential in better alignment with the Alaska $\delta^{18}O$ records (Fig. 6). It also slightly amplifies glacial-interglacial δ^2H change, as there were more graminoids during the glacial period than the Holocene, and also indicates that changes in $\delta^2H_{precipitation}$ likely began prior to the 11.6 ka step change.

The propogation of analytical and calibration uncertainty results in fairly large uncertainty for the calculated $\delta^2H_{precipitation}$ and temperature reconstruction values. Analytical uncertainty of δ^2H measurements is excellent, with a pooled standard deviation of replicate measurements of 1.3‰ (Table S3). After consideration of the changing vegetation assemblages and the assumed end member fractionation values and their uncertainty, the 95% confidence interval on the reconstructed $\delta^2H_{precipitation}$ measurements is ±22‰, similar to the root square error for *n*-acids and *n*-alkanes conversions globally (McFarlin et al., 2019). This level of uncertainty is on the same order of magnitude as the observed changes in δ^2H_{wax} over the Lake E5 record. The 25%–75% CI for $\delta^2H_{precipitation}$ is ±9‰ and is shown in the figures. After converting these values to temperature and assessing the anomaly from present day, we find that the temperature change has a 95% confidence interval of ±8 °C. The 25-75% CI for temperature is ±3.5 °C.

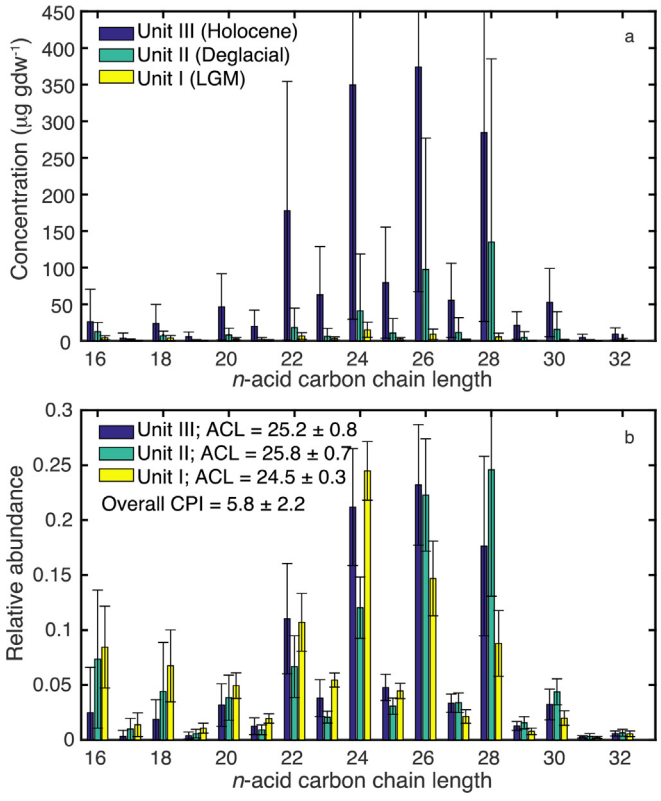

Fig. 4. Leaf wax *n*-acid concentrations and distributions from Lake E5 sediments. Colors correspond to the three identified sedimentary units, which relate to the LGM (yellow), the last deglacial period (teal), and the Holocene (blue). a) *n*-acid concentrations s. b) Fractional abundance of *n*-acids relative to the C_{16}–C_{32} total. Error bars signify 1 standard deviation among samples of each unit. (For interpretation of the references to colour in this figure legend, the reader is referred to the Web version of this article.)

4. Discussion

4.1. Climatic interpretation of $\delta^2H_{precipitation}$

Due to the strong relationship between air temperature and $\delta^2H_{precipitation}$ in the Arctic (Dansgaard, 1964) and at the Toolik Field Station (Fig. 3), $\delta^2H_{precipitation}$ is a useful proxy for reconstructing past air temperature (Pautler et al., 2014; Klein et al., 2015; Porter et al., 2019). Changes in moisture source that resulted from changes in Arctic sea ice cover, site continentality, or prevailing wind directions could impart effects on $\delta^2H_{precipitation}$ at Lake E5, but we posit that such effects are secondary to the control of condensation temperature at the site, and that they in fact contribute to the empirical relationship between temperature and $\delta^2H_{precipitation}$ that we observe in modern monitoring. The Arctic Ocean, Bering Sea, and North Pacific are the dominant sources of moisture to the North Slope of Alaska (Mellat et al., Submitted). Precipitation originating in the Gulf of Alaska is more ^2H-depleted than Arctic Ocean or Bering Sea moisture sources because of a larger rainout trajectory and orographic rainout as airmasses move

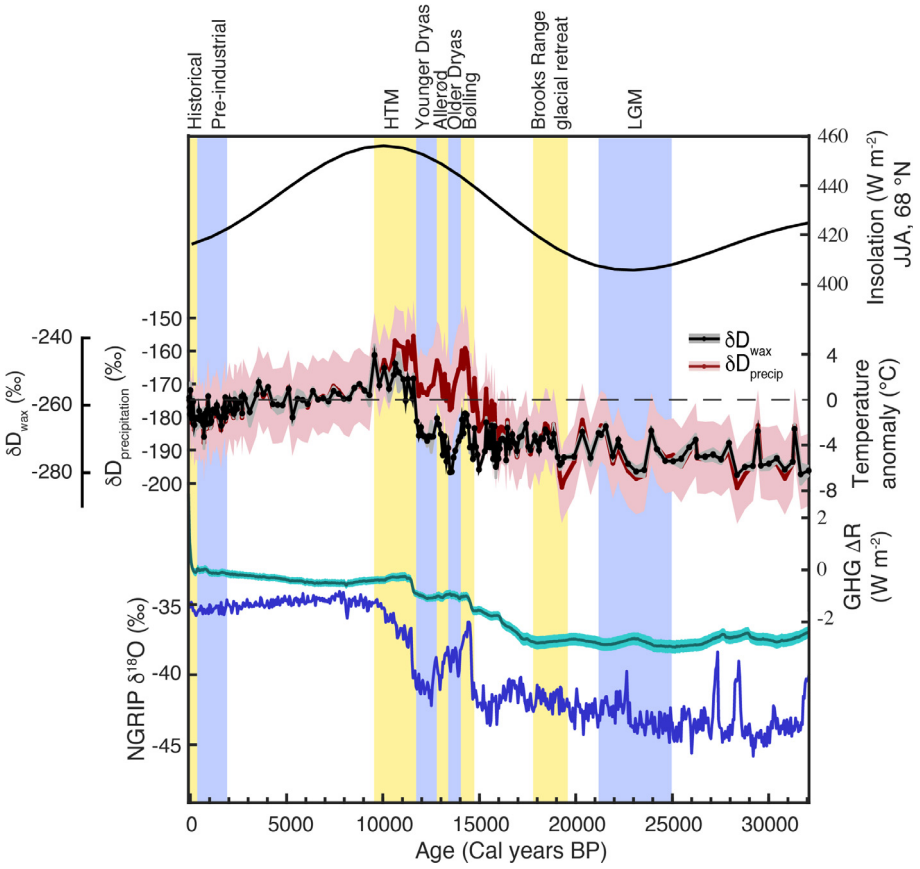

Fig. 5. A comparison between summer (JJA) insolation (Laskar et al., 2004), Lake E5 δ^2H_{wax} (black) and inferred $\delta^2H_{precipitation}$ and temperature anomalies with 75% and 25% confidence bounds shown for temperature estimates (red with pink shading), relative greenhouse gas radiative forcing from CO_2, CH_4, and N_2O (Köhler et al., 2017), and the NGRIP $\delta^{18}O$ record (Andersen et al., 2004). (For interpretation of the references to colour in this figure legend, the reader is referred to the Web version of this article.)

across the Alaska interior (Lachniet et al., 2016; Putman et al., 2017; Bailey et al., 2019). The more negative δ^2H signature of southern airmasses occurs despite the Arctic Ocean being ~15‰ ^2H-depleted relative to the North Pacific (Schmidt et al., 1999). A smaller-scale and reversed precipitation isotope gradient is also observed across the North Slope, wherein Arctic Ocean-sourced moisture becomes ^2H-depleted as it travels southeastward (Gaglioti et al., 2017). Although these "source effects" are influential, seasonal changes in moisture source are largely controlled by sea ice coverage, which together with air temperature, gives rise to a strong seasonal cycle in $\delta^2H_{precipitation}$ at Lake E5 (Daniels et al., 2017) and a positive correlation between air temperature and $\delta^2H_{precipitation}$ (Fig. 3). Because these seasonal changes are analogous to changes over glacial-interglacial time scales, the modern temperature-$\delta^2H_{precipitation}$ relationship offers a transfer function for approximating past temperature in northern Alaska.

The utility of the modern temperature-$\delta^2H_{precipitation}$ relationship is further supported by an investigation of isotope-enabled climate model simulations of the past 20 ka which shows that the relationship between temperature and $\delta^2H_{precipitation}$ has remained approximately constant since the LGM (Fig. S5). The modeled modern slope is substantially lower than the observed relationship between temperature and $\delta D_{precipitation}$, but the modeled slopes remains stable during and since the LGM, reflecting the approximate stationarity of the temperature-$\delta^2H_{precipitation}$ relationship over this interval and adding confidence in the temperature interpretation of the $\delta^2H_{precipitation}$ record. Temperature anomalies are calculated using the observed modern slope of 3.4‰ $°C^{-1}$, which is similar to the slope reported across a number of Arctic North American sites (3.1‰ per °C Porter et al., 2016).

Estimates of temperature change from δ^2H_{wax} are also influenced by the seasonality of precipitation used for plant leaf wax synthesis. Although tundra plant growth is constrained to the summer growing season, the water used in their biosynthesis has been linked to both warm and cold season precipitation sources (Welker et al., 2005; Jespersen et al., 2018). Wilkie et al. (2012) suggest a bias toward use of remnant autumnal precipitation in supporting spring leaf production, whereas others have used terrestrial wax $^2H/^1H$ as a proxy for summer precipitation (Thomas et al., 2012; Porter et al., 2016). In our study area, approximately 60% of the annual precipitation falls during JJA (Cherry et al., 2014); Daniels et al. (2017) identify seasonally changing soilwater isotopic composition throughout the growing season and suggest that although cold season precipitation can contribute to biosynthesis, summer rainfall is the most important hydrogen source for leaf wax production. Given the mixture of seasonal precipitation utilized by tundra plants, the potential for changing growing season lengths, and the strong event-based correlation between temperature and $\delta^2H_{precipitation}$ across the seasons, we use the annual temperature-$\delta^2H_{precipitation}$ relationship to translate our δ^2H_{wax} measurements into summer-biased temperature change estimates.

The seasonal nature of the leaf wax proxy is exemplified in a direct comparison with the lacustrine alkenone record from Lake E5 (Fig. 7; Longo et al., 2020). Alkenone production was observed to be greatest early in the spring in Arctic lakes (Longo et al., 2016), and as such, the alkenone-inferred temperatures are sensitive to spring ice cover and cold-season conditions. During the deglacial period, both alkenone and δ^2H_{wax} suggest warming of a similar

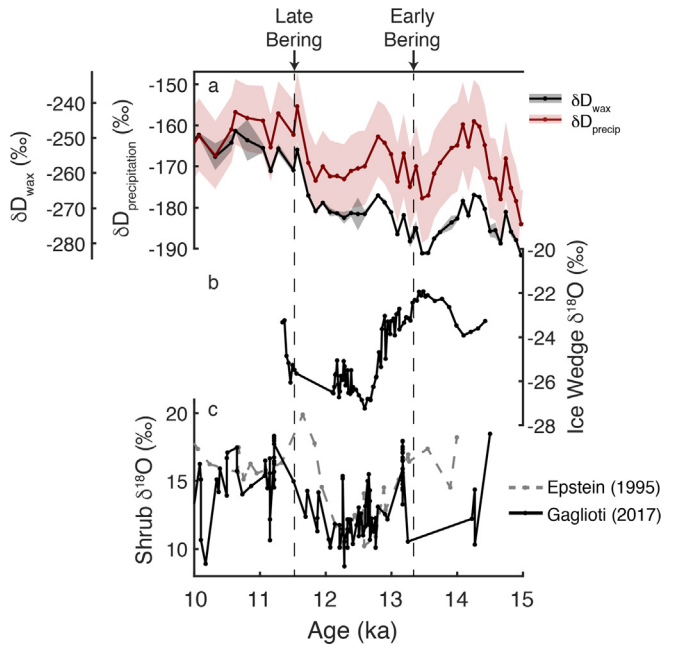

Fig. 6. Comparison of Alaska water isotope records during the Younger Dryas interval demonstrating that the vegetation-based correction brings the Lake E5 D/H record into better agreement with other nearby isotope records. a) Ice-volume corrected δ^2H_{wax} from Lake E5 (black with gray shading showing 1σ of analytical uncertainty), and the inferred $\delta^2H_{precipitation}$ following application of the pollen-guided fractionation factors (red with pink shading showing 25 and 75% confidence intervals of the monte carlo simulation); b) Ice wedge $\delta^{18}O$ values from Barrow, Alaska (Meyer et al., 2010); c) Salix (willow shrub) cellulose $\delta^{18}O$ from the North Slope of Alaska (Epstein, 1995; Gaglioti et al., 2017). Timing of the dual-phase opening of the Bering Strait is also shown (Pico et al., 2020). (For interpretation of the references to colour in this figure legend, the reader is referred to the Web version of this article.)

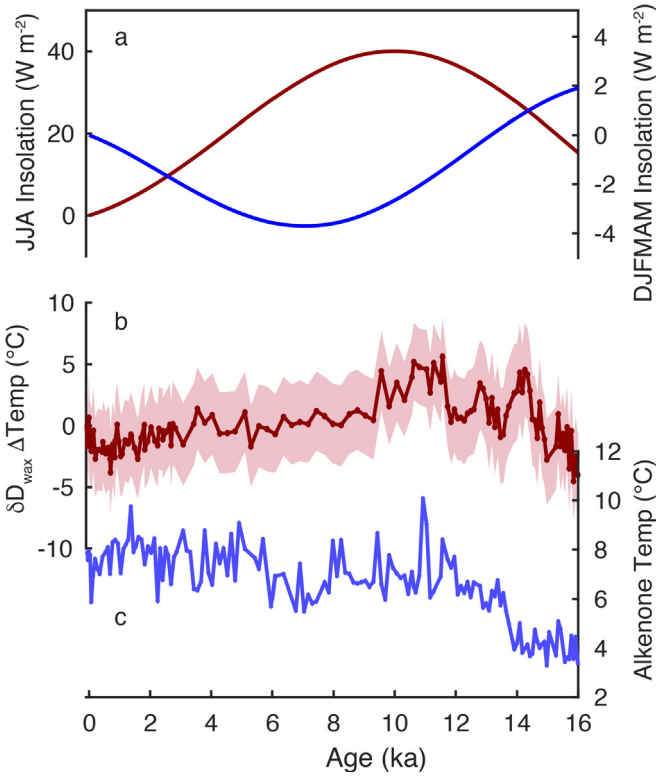

Fig. 7. Comparison of Lake E5 alkenone- and δ^2H_{wax}-inferred temperature changes. a) Deviations from present day in mean insolation at 68 °N for summer (JJA, red) and the cold season (DJFMAM, blue). b) Temperature anomaly based on the leaf wax $^2H/^1H$ proxy, with 25% and 75% confidence interval. c) Alkenone-derived temperatures (Longo et al., 2020). (For interpretation of the references to colour in this figure legend, the reader is referred to the Web version of this article.)

magnitude, albeit with some differences in the timing and the nature of abrupt climate events. Both proxies exhibit an early temperature maximum in the early Holocene, after which they diverge substantially, with alkenones showing a general warming trend, particularly in the last 8 kyr, whereas δ^2H_{wax} showing a cooling trend over the same interval. This contrast signifies that the temperatures of different seasons are responding to different drivers over the Holocene. Namely, cold-season temperatures appear to be sensitive to winter insolation and greenhouse gas forcing (Longo et al., 2020), while summer temperatures show a stronger relationship with summer insolation.

4.2. Glacial-interglacial climate change

The vegetation-corrected $\delta^2H_{precipitation}$ and inferred temperatures at Lake E5 exhibit distinct glacial-interglacial structure (Fig. 6), with LGM δ^2H_{wax} approximately 10–15‰ more negative than today. This magnitude of change is similar to that observed in leaf waxes in the Yukon Territory (Pautler et al., 2014). Based on the Monte Carlo simulations, inferred temperatures during the LGM were approximately 4 °C lower than during the Historical Period (1900-2014 CE), with individual iterations ranging from 10 °C cooler to 2 °C warmer. Compared to the Pre-industrial period (PI; 2–0.1 ka), LGM temperatures were just 3 °C cooler (Monte Carlo range: −8 to +3 °C). The estimated ΔT of -4 °C for the LGM is less severe than LGM cooling observed in Greenland, northern Europe, and other parts of North America (Fig. 8), but is within the range of previous estimates for Eastern Beringia (Table S4, and references therein). For Beringia, 18 warm-season temperature reconstructions have an average LGM temperature change of −4 °C. The six sites fringing the Laurentide Ice Sheet, combined with Greenland borehole temperature, had an average temperature change of −18 °C. Asia and Europe saw ΔT of −3 and −6 °C, respectively. We examined the ensemble output from the Paleoclimate-Model Intercomparison Project 3 (PMIP3) and find that the model results generally agree well with proxy reconstructions (Fig. 8), simulating strongest cooling around the Laurentide and Greenland Ice Sheets and relatively weak cooling over Beringia. The model ensemble slightly overestimates cooling in mid- to high-latitude Europe. Additional proxy reconstructions from Asia are needed to evaluate the spatial pattern of LGM temperature change there. The mild conditions reconstructed for Beringia may have been important for maintaining the highly-productive mammoth-steppe tundra (Zimov et al., 2012) and sustaining human occupation of Beringia through the LGM (Goebel et al., 2008; Vachula et al., 2019).

Our finding of relatively weak summertime cooling during the LGM could support the hypothesis that the orographic effect of the Laurentide Ice Sheet was to steer relatively warm air into the region (Otto-Bliesner et al., 2006; Briner and Kaufman, 2008; Bartlein et al., 2011). Other mechanisms may have also contributed to maintaining the mild summer climate. For example, Löfverström and Liakka (2016) suggest that reduced cloud cover during the LGM allowed more downwelling shortwave radiation to reach the land surface, further contributing to warmth in Alaska, an effect that would be most impactful during summer. Using a compilation of sea surface temperatures, Rae et al. (2020) show that the North Pacific surface ocean was 2 °C warmer during the LGM than at present, owing to strengthened meridional heat transport in the

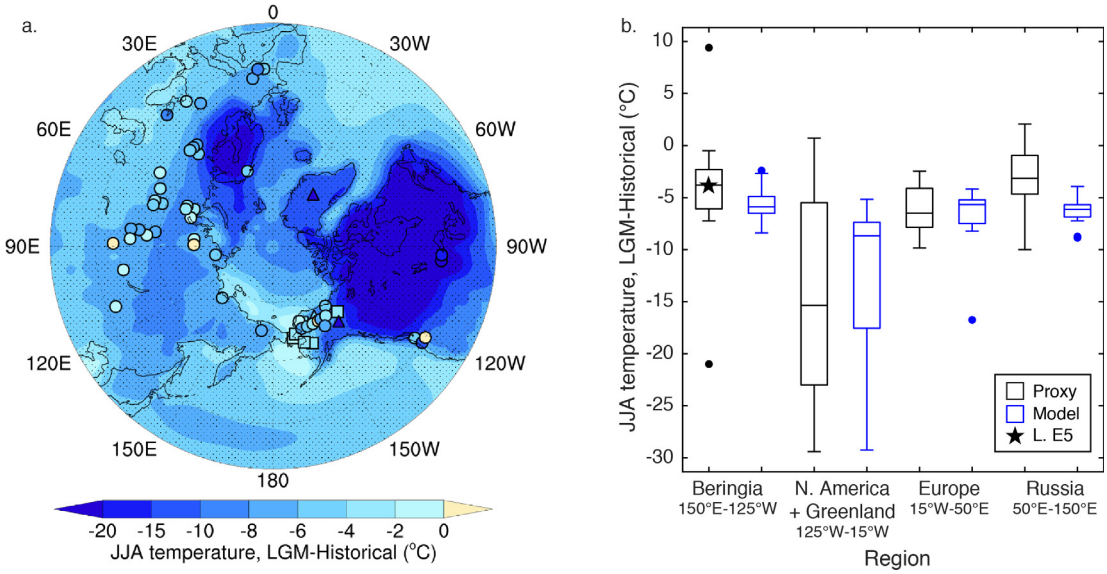

Fig. 8. Data-model comparison of LGM warm-season temperature anomalies across the Arctic. **a.** PMIP3 multi-model ensemble average JJA temperature anomalies relative to the historical period (1900-2000 CE) overlain by published LGM temperature reconstructions based on pollen (circles), insects (squares), and geochemistry (triangles) (Table S4). **b.** LGM temperature anomalies in proxies and the multi-model means in four sectors of the Arctic. Model data are extracted from gridcells within 2° of proxy sites, and do not include ice-sheet or ocean cells, with the exceptions of the Greenland and Norway locations, for which ice-free grid cells are not available in models.

Pacific. This oceanic warming may have had regional impacts on surface temperature. Furthermore, in the CCSM3 simulations (Fig. 8), mild LGM temperatures are localized over the Bering Strait, implying that exposure of the Bering Land Bridge, through its effects on surface energy balance (Bartlein et al., 2015), may have partially offset LGM summertime cooling in the immediate Bering Strait vicinity. West of the Bering Strait, moderating effects of the ice-sheet orography and land-bridge were less pronounced, with LGM summer temperatures at Lake El'gygytgyn in Far East Russia 8-9 °C colder than present (Melles et al., 2012), nearly double the global average ΔT of -4.9 °C (Shakun and Carlson, 2010). Thus, while much of North America, Europe, and Asia experienced enhanced LGM cooling due to continental ice sheet and sea ice growth and possible redirection of polar air masses into those regions (Miller et al., 2010), Beringia-specific changes in land exposure and the advection of relatively warm air dampened LGM cooling, resulting in regionally distinct expressions of Arctic Amplification.

There are few records of winter LGM climate with which to compare the summer reconstructions. Pollen-based inferences suggest comparable magnitude of winter and summer temperature change in Alaska (Viau et al., 2008), although these authors note that deconvolving seasonal signals from pollen is tenuous in the region. To the southeast of our site, in central Yukon Territory and in close proximity to the Laurentide and Cordilleran Ice Sheets, Pautler et al. (2014) analyzed multiple biomarkers and found that the winter-biased proxy showed a greater LGM temperaure change than the warm-season proxy. Porter et al. (2016) report that annual and cold-season temperatures of the Yukon were ~14–21 °C below present day but did not independently constrain warm season temperatures. In Siberia, pollen spectra suggest that LGM cooling was approximately twice as strong in winter as summer (Wetterich et al., 2011). Likewise there is a strong seasonal difference in LGM climate change in the North Atlantic (Denton et al., 2005), in large part because the sea ice feedbacks are stronger in winter than in summer. As mentioned previously, ice wedges and lacustrine alkenones are two approaches to investigate past winter conditions in Beringia. Currently, records of these proxies are found from the late glacial through the Holocene (Meyer et al., 2010; Longo et al., 2020), and reconstructions extending through the LGM may help decipher how summer and winter climate drivers differed.

4.3. Rapid changes during the glacial termination

$\delta^2H_{precipitation}$ at Lake E5 generally tracks changes in summer insolation. Increasing $\delta^2H_{precipitation}$ is evident as early as 23.1 ± 0.9 ka, and steady, more substantial increase began at 16.9 ± 0.5 ka, coinciding with increased radiative forcing from greenhouse gases (Köhler et al., 2017), and culminating in a brief periods of rapid rise at 14.8 ± 0.3 ka and again at 11.6 ± 0.2 ka. Inferred temperatures rose by ~8 °C (Monte Carlo range: +6 to +10 °C) from the LGM to an early Holocene thermal maximum (HTM) from 11.6–9.5 ka, then cooled steadily until the PI era. While the overall correspondences between temperature, greenhouse gas forcing, and summer insolation are strong, we observe several intervals of abrupt warming and cooling during the glacial termination (Fig. 5).

Early in the glacial termination, there was rapid δ^2H_{wax} increase from 19.3 ± 0.7 ka to 18.9 ± 0.7 ka. The magnitude is estimated to be equivalent to ~4 °C (Monte Carlo range: +0 to +8 °C). The warming can help explain suggestions of rapid glacier retreat in the nearby Brooks Range mountains dated to 19 ka (Pendleton et al., 2015). The causes for this early, strong warming have been enigmatic, and include increasing summer insolation and a maximum in the effect of the LIS on atmospheric flow (Pendleton et al., 2015), but it is unclear how these processes would produce the abrupt, short-lived warming observed in the δ^2H_{wax} record. We propose an oceanic driver of this warming event. Ventilation ages of the North Pacific document an invigorated PMOC beginning at 19 ka (Fig. 9) which would have increased the total northward heat transport in the Pacific by approximately 0.7 PW, with the greatest amount of resultant ocean warming near the Gulf of Alaska and Bering Strait (Okazaki et al., 2010). Model simulations indicate that PMOC intensifies in response to AMOC collapse (Hu et al., 2012), for example during HS1, due to reduced evaporation and increased sea surface salinity in the North Pacific. We note, however, that empirical evidence for PMOC intensification predates the reduction in AMOC marking the onset of HS1 (Fig. 6; McManus et al., 2004; Okazaki

et al., 2010). While the cause of the potential PMOC invigoration remains uncertain, the increased northward oceanic heat transport in both oceans just prior to HS1 likely contributed to warming from 19–18 ka in Alaska, while subsequent HS1 cooling may have been suppressed in Alaska by sustained PMOC activity.

Abrupt δ^2H_{wax} increases at 14.8 ± 0.3 and 11.6 ± 0.2 ka in the Lake E5 record (Figs. 5 and 3) correspond with the onset of the Bølling interstadial and the termination of the Younger Dryas, indicating Arctic Alaskan temperature change was positively correlated with changes in the North Atlantic during the latter part of the deglaciation. Reconstructed temperature change was approximately +4 °C (Monte Carlo range: +1 to +8 °C) at the Bølling onset and +3 °C (Monte Carlo range: −4 to +8 °C) over the YD termination, much smaller than the 9 °C changes reconstructed over Greenland (Severinghaus and Brook, 1999). Both events are driven by strengthening and possible "overshoot" of AMOC (Liu et al., 2009). While BA-YD fluctuations are seen in oceanographic records of the Bering Sea (Kühn et al., 2014) and Gulf of Alaska (Praetorius and Mix, 2014), the much larger surface warming observed at Greenland indicates that the surface temperature response to AMOC variability is weaker in continental Beringia. Furthermore, comparison of the Lake E5 $\delta D_{precipitation}$, which records summer variability, with ice wedge isotopes in Barrow, AK, which record winter conditions, suggests that the BA-YD oscillation impacted all seasons, but was expressed most strongly in the winter season (Fig. 6). Nevertheless, the two events encompass most of the deglacial temperature increase at Lake E5. The Bølling-onset inferred here coincides with expansion of graminoid sedges and precedes a vegetation shift from herb steppe tundra to deciduous shrub tundra between 13.9 and 12.6 seen in Brooks Range-area pollen records (Oswald et al., 1999; Mann et al., 2002; Abbott et al., 2010). We speculate that the temporary expansion of sedges was in part responsive to increased moisture availability during the BA, and subsequent warming towards the end of the YD promoted the expansion of *Betula* and other shrubs (Fig. S3). The expansion of shrubs would have accelerated deglacial warming by increasing the surface energy balance of the Alaska land surface by 2–3 W m^{-2} (Lynch et al., 1999), similar to changes occurring today (Sturm et al., 2001; Elmendorf et al., 2012). The relatively low-resolution sampling of the pollen make it difficult to determine if the isotopic proxy and vegetation assemblages have different response times to climate change.

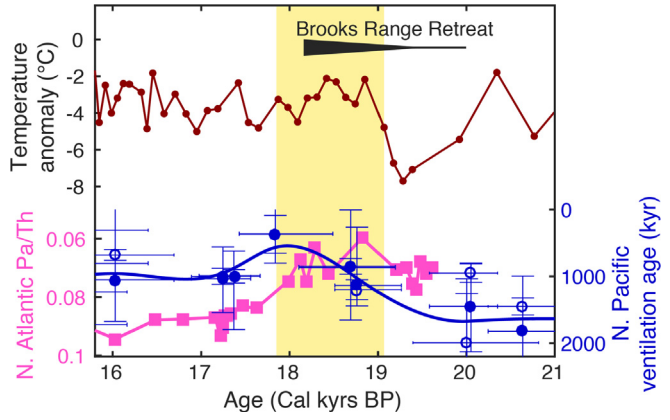

Fig. 9. Comparison of early deglacial warming at Lake E5 and marine indicators of PMOC and AMOC intensity. Lake E5 temperature anomaly (red) is based on δ^2H_{wax} relative to the historical period. N. Pacific ventilation ages (blue) reflect PMOC intensity (Okazaki et al., 2010), while Pa/Th from the Bermuda Rise (magenta) is an indicator of AMOC intensity (McManus et al., 2004). Also shown is the period of rapid glacier retreat in the Brooks Range mountains near Lake E5 (Pendleton et al., 2015). (For interpretation of the references to colour in this figure legend, the reader is referred to the Web version of this article.)

The pre-YD warm interval occurred in two phases, interrupted by a short-lived cool period at approximately 14 ka correlating with the Older Dryas interval recognized from the North Atlantic (Grootes and Stuiver, 1997; Mangerud et al., 2017) region as well as the North Pacific (Kienast and McKay, 2001). Following this, δ^2H_{wax} increased, with inferred temperatures increasing by 3 °C (+1 to +4 °C) between 13.5 ± 0.3 and 12.8 ± 0.2 ka, marking the onset of a warm interval correlating with the Allerød Interstadial. In contrast to the NGRIP isotope record which suggests cooling across the B-A (Andersen et al., 2004) the Bølling and Allerød periods are of comparable temperatures at Lake E5. This contrast is also recognized in Southern Alaska (Hu et al., 2006), and could arise from processes local to Beringia, such as the flooding of the Bering Land Bridge, which possibly enhanced Allerød warming in the area.

The submergence of the Bering land bridge during the late deglacial likely had profound impact on Beringia climate (Bartlein et al., 2015). The Pacific and Arctic Oceans became connected between 11 and 13.4 ka (Elias et al., 1996; Keigwin et al., 2006; England and Furze, 2008; Jakobsson et al., 2017), although the timing is not precisely known (Clark et al., 2014). Geophysical modeling of regional ice sheets and isostatic adjustment suggests the possibility of a two-phase land bridge inundation, with the first Pacific-Arctic connection forming ~13.3 ka, followed by a more substantive flooding event ~11.5 ka, with these periods bracketing an approximate intermission in local sea level change (Pico et al., 2020). Their model identifies regional isostatic rebound from 13 to 11.5 ka, driven by mass loss from the Cordilleran and western Laurentide Ice Sheet, as the principal driver of the hiatus in Bering Strait flooding. If the summer warming signal at 13.4 ka in the Lake E5 δ^2H_{wax} record represents the broader region, this may have provided an important mechanism contributing to retreat of the Cordillaran Ice Sheet or western Laurentide Ice Sheet at that time.

We tested the impacts of Bering submergence using idealized experiments in CCSM3 by simulating Beringia surface temperatures under Bering Strait open and closed scenarios (BSO and BSC) and under 15 ka (deglacial) and 0 ka (interglacial) climate boundary conditions. Upon opening of the strait we observe little change, or cooling in the annual temperature immediately over the Bering Sea. However, moving away from the strait, the effect is reversed, with 0.5–1.5 °C warming over interior Alaska (Fig. 10). The warming effect is stronger under interglacial climate conditions. Under late glacial boundary conditions, the warming impact of Bering submergence is strongest over southeast Alaska. Thus, although the simulations are idealized and do not test the climate impacts of initial strait opening, they provide qualitative support for the idea that increased Bering Strait throughflow warms interior Alaska, despite the fact that the marine transgression resulted in summer cooling in the immediate vicinity of the Bering Strait (Bartlein et al., 2015). An early opening of the Bering Strait (~13.3 ka) may therefore be linked to the enhanced Allerød warming signal at Lake E5, whereas a late opening (~11.5 ka) may have contributed to YD-termination warmth and a sustained early Holocene warm period in Eastern Beringia.

Abrupt warming events at 13.5 ka and 11.6 ka bracket a Younger Dryas cool interval. Across Eastern Beringia, indications of YD climate anomalies variably are absent (Kokorowski et al., 2008; Kurek et al., 2009a, 2009b), demonstrate wintertime cooling (Meyer et al., 2010), demonstrate summertime cooling (Engstrom et al., 1990; Hamilton, 2003; Mann et al., 2010; Gaglioti et al., 2017), or suggest a return to arid conditions (Abbott et al., 2000; Mann et al., 2002). In Lake E5, δ^2H_{wax} decreased by 10‰ beginning at 12.8 ± 0.2 ka, equivalent to approximately 3 °C of summer cooling.

The YD climate reversal is typically attributed to surface water

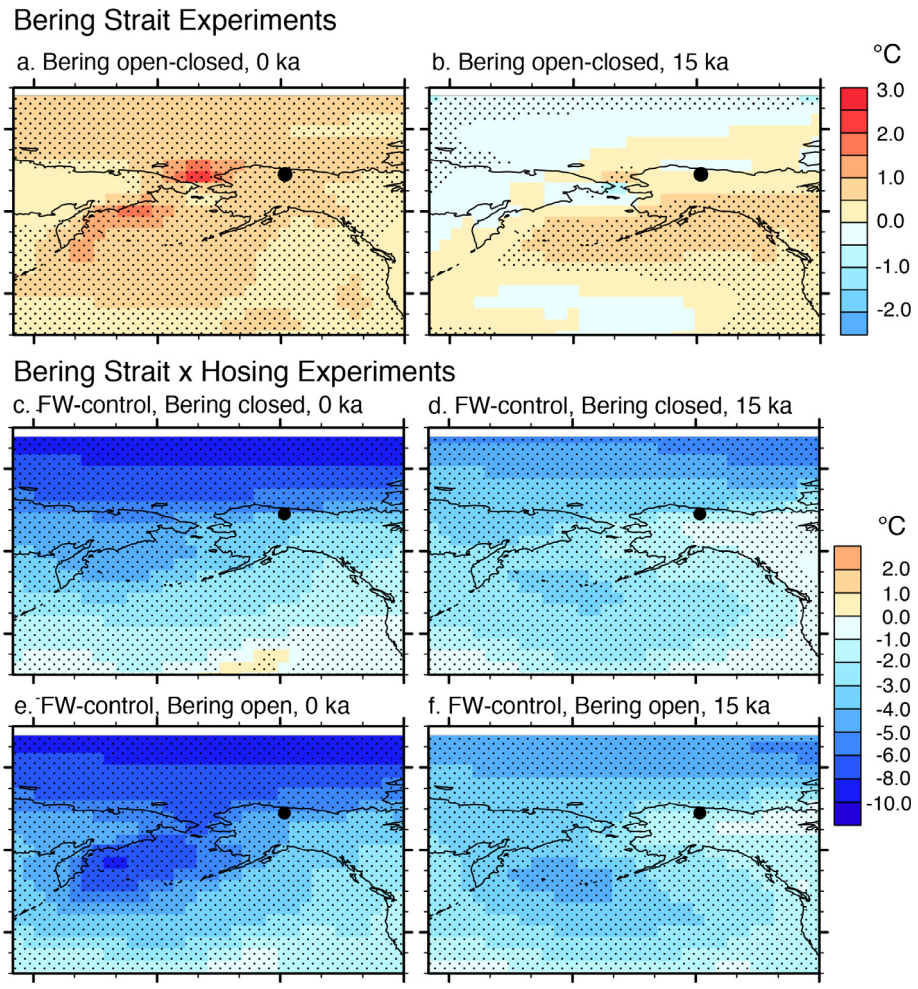

Fig. 10. Mean annual surface temperature anomalies in Beringia in CCSM3 experiments. Stippling represents anomalies that are statistically significant at the p = 0.05 level according to a *t*-test. **a.** and **b.** Mean annual temperature anomalies between simulations with open and closed Bering Strait under present-day (1990 A.D.) and 15 ka boundary conditions, respectively; **c.** and **d.** Mean annual temperature anomaly between hosing experiments and control simulations under closed Bering Strait conditions for 0 ka and 15 ka; **e.** and **f.** Same as **c.** and **d.** but with an open Bering Strait.

freshening in the North Atlantic, slowing of AMOC, and reduction of northward oceanic heat transport into the high northern latitudes. We tested the impacts of these processes on Beringian climate using idealized freshwater hosing experiments in the CCSM3 by simulating AMOC collapse under the same scenarios as the Bering Strait experiments (Fig. 10). Under deglacial boundary conditions, AMOC collapse results in a range of cooling of 1–3 °C in Alaska for a fully-open strait and 0-2 °C when the strait is still closed. Under present-day (0 ka) boundary conditions, the temperature sensitivity to North Atlantic freshwater forcing is approximately double that of the deglacial simulations for both BSO and BSC scenarios, suggesting that a weakened AMOC has a much larger impact on Arctic Alaskan climate when the global climate is warmer. In addition, the prediction that the magnitude of cooling is ~50% weaker when the Bering Strait is closed, may help explain the weak expression of HS1 in Lake E5 sediments.

4.4. Climate of the holocene

The most prominent feature of the Holocene is a $\delta^2H_{precipitation}$ and inferred-temperature maximum from ~11.6 to 9.5 ka (Fig. 5), followed by a gradual cooling until the PI period. The inferred $\delta^2H_{precipitation}$ was 19‰ higher during this early Holocene Thermal Maximum (HTM) compared to PI period, while temperatures averaged 6 °C warmer (Monte Carlo range: +0 to +10 °C). Compared to the Historical period, $\delta^2H_{precipitation}$ during the HTM was 16‰ higher and temperatures averaged 4 °C warmer (Monte Carlo range: −1 to +10 °C). The timing of the HTM is approximately synchronous with peak NH summer insolation (Fig. 5), and occurs slightly earlier than in the Yukon Territory (Porter et al., 2019) and locations further east (Kaufman, 2004). The termination of the HTM occurs abruptly, with ~2 °C of cooling at 9.5 ± 0.2 ka, followed by gradual cooling that follows trends in summer insolation.

While most records from the region agree that early Holocene temperatures were as warm or warmer than present, the inferred magnitude of Holocene cooling at Lake E5 exceeds some but not all estimates for Alaska. HTM summer temperatures along the Chukchi Sea coastal region were 4–6 °C warmer than present, based on fossil beetle assemblages (Elias et al., 1996), in good agreement with the δD_{wax} inference. Lacustrine chironomid records from Zagoskin Lake near the Bering Strait (Kurek et al., 2009a) and Trout Lake in the Yukon Territory (Irvine et al., 2012) suggest temperatures were 2-3 °C warmer during the HTM, somewhat smaller in magnitude, but within the uncertainty of the δ^2H_{wax} inference. At Trout Lake, most of this cooling occurred at 9.6 ka, synchronous to the stepped δ^2H_{wax} decline at Lake E5. Holocene temperatures were approximately stable at Burial Lake in northwest Alaska (Kurek et al., 2009a) and at Hanging Lake in the northern Yukon (Kurek

et al., 2009b). The absent or more subtle cooling signal seen in the chironomids compared to δ^2H_{wax} or beetles could result from limitations in the various proxy interpretations. Alternatively, reduced temperature variability at Zagoskin and Burial Lakes have been attributed to their proximity to the ocean (Kurek et al., 2009a); given the more continental location of Lake E5, this suggests that the interior regions of eastern Beringia experienced a relatively amplified Holocene cooling compared to these other sites.

The leaf wax $^2H/^1H$ record from Lake E5 generally agrees with Holocene declines in lacustrine $\delta^{18}O$ recorded at nearby Schrader Pond in Northeast Alaska (Broadman et al., 2020), as well as a number of sites in southern and central Alaska (Anderson et al., 2001; Vachula et al., 2017). Broadman et al. (2020) suggest that the general decrease in $\delta^{18}O$ values across Alaska is driven in part by expansion of Arctic sea ice. However, there is a late Holocene increase in cellulose $\delta^{18}O$ at St. Matthews Island in the central Bering Sea (Jones et al., 2020), interpreted to result from declining winter ice cover in the Bering Sea. More records of sea ice are needed to elucidate if Arctic and Bering sea ice histories are decoupled or if the apparent difference results from different seasonal expressions of the $\delta^{18}O$ sea ice responses at continental and island sites. The continental sites, which together document cooling and drying of Beringia climate over the Holocene, with a particular bias towards summer conditions, contrast with the Lake E5 alkenone record which records a winter/spring warming signal over the Holocene in response to increasing cold-season insolation and greenhouse gasses (Longo et al., 2020). The contrasting wintertime warming signal is regionally corroborated by ice wedge isotopes in the Yukon (Holland et al., 2020) as well as the retreating winter sea ice cover in the Bering Sea (Jones et al., 2020). The Lake E5 record shows that after brief warm periods at ~5.6 ± 0.2 ka and from 4.0 to 3.5 ka, cooling re-intensified from 4 to 0.1 ka, which is roughly synchronous with the expansion of alpine glaciers in the Brooks Range (Badding et al., 2013). Temperatures were more stable during over the last 2000 years (Fig. 11), but the median of the monte carlo simulation still exhibits cooling at a rate of ~0.6 ± 0.2 °C per millennium, exceeding the average pan-Arctic late Holocene cooling of 0.22 °C per thousand years (Kaufman et al., 2009).

The Lake E5 $\delta^2H_{precipitation}$ record contextualizes ongoing Alaska warming in the prism of climate changes of the past ~32 kyr. Fig. 11 shows that modern (coretop) leaf waxes from the historical era at Lake E5 are ^2H-enriched relative to the PI average by 5.2 ± 0.8‰, equating to ~2 °C of warming (Monte Carlo range: −1 to +5 °C). The amplitude of post-industrial warming we reconstruct at Lake E5 is similar to the 2.5 °C of JJA warming apparent in the CRUTEM4 instrumental database for Northern Alaska (Jones et al., 2012) and the 2 °C rise in mean annual temperature inferred from the nearby McCall glacier ice core $^{18}O/^{16}O$ ratios (Klein et al., 2015). Furthermore, whereas, Porter et al. (2019) show, based on $^{18}O/^{16}O$ in ground ice, that recent warming in Central Yukon has surpassed peak early-Holocene warmth, this is not the case at Lake E5. The $\delta^{18}O$ values in diatoms at nearby Schrader Lake decline during the Holocene but do not exhibit a reversal to HTM levels (Broadman et al., 2020). Nonetheless, the isotope-inferred warming at Lake E5, in conjunction with the instrumental observations, indicate that recent temperature increase in northern Alaska exceeds the +1.4 °C pan-Arctic temperature change between the pre-industrial period and today (Kaufman et al., 2009). This amplified warming contrasts with the spatial pattern of temperature change across the deglaciation, when Beringian warming was smaller than other parts of the Arctic. The contraction of winter and summer sea ice in the adjacent Chukchi Sea (Serreze et al., 2007; Stroeve et al., 2012) and the expansion of shrubs into low tundra biomes (Sturm et al., 2001; Elmendorf et al., 2012; Buchwal et al., 2020) are likely feedbacks amplifying recent warming in northern Alaska.

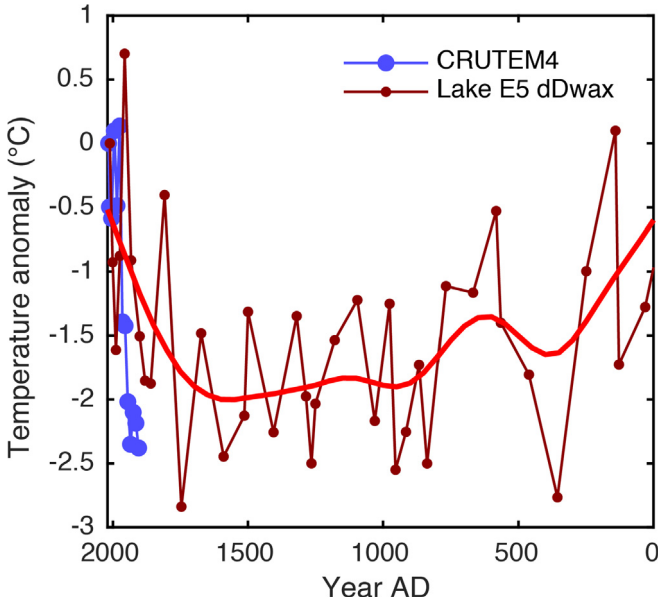

Fig. 11. Lake E5 δ^2H_{wax}-inferred temperature anomalies over the past 1000 years (red, with smoothing spline) and CRUTEM4 instrumental observations from Northern Alaska (blue). (For interpretation of the references to colour in this figure legend, the reader is referred to the Web version of this article.)

5. Conclusions

A new record of Eastern Beringia paleoclimate provides evidence for a relatively mild LGM and a series of abrupt climate transitions during the deglacial period, with rapid warming intervals observed at 19 ka, 14.8 ka, 13.4 and 11.6 ka. Furthermore, data-model comparisons demonstrate that the magnitude of past Arctic amplification in this region has evolved from the last glacial period to today. In particular, whereas muted LGM cooling in Beringia indicates strong ameliorating effects of ice sheet orography and possibly enhanced continentality, the Holocene and modern changes are amplified relative to other Arctic sites, which we speculate is due to surface feedbacks including recent sea ice decline and shrub expansion in conjunction with the removal of factors such as the LIS which dampened regional temperature change during the deglacial. These results predict that Arctic Alaskan temperatures will continue to warm more rapidly in the future than other sectors of the Arctic.

Declaration of competing interest

The authors declare that they have no known competing financial interests or personal relationships that could have appeared to influence the work reported in this paper.

Acknowledgments

We thank Rafael Tarozo for laboratory assistance.This work is partially supported by National Geographic grant 9397-13 (Y.H.), and National Science Foundation grants PLR-1503846 (Y.H., J.M.R.), PLR-1504069 (C.M.) and DEB-1026843 (ARC-LTER), and DBI-0923571 (J.M.W.) and a National Ocean Sciences Accelerator Mass Spectroscopy Graduate Student Internship (W.M.L.). A.H. is supported by the Regional and Global Model Analysis (RGMA) component of the Earth and Environmental System Modeling

Program of the U.S. Department of Energy's Office of Biological & Environmental Research Cooperative Agreement # DE-FC02-97ER62402, and the NSF. The National Center for Atmospheric Research is sponsored by the NSF. This research used resources of the National Energy Research Scientific Computing Center, a DOE Office of Science User Facility supported by the Office of Science of the DOE under Contract No. DE-AC02-05CH11231.

Author statement

W. C. Daniels: Conceptualization, Investigation, Data curation,Writing-original draft preparation, Writing-review and editing, visualization, J. M Russell: Conceptualization, Methodology, Resources,Writing-Original draft preparation, Writing-review and editing, Supervision, Funding acquisition, C. Morrill: Conceptualization, Software, Resources, Writing-Original draft preparation, Writing-review and editing, Visualization; Project administration, Funding acquisition, W. M. Longo: Investigation, Data curation, Writing-review and editing; Funding acquisition, A. E. Giblin: Supervision, Writing-review and editing, Funding Acquisition, P. Holland-Stergar: Investigation, J. M. Welker: Conceptualization, Investigation, Project administration, Funding Acquisition, X. Wen: Software, Writing-review and editing. A. Hu: Conceptualization, Software, Writing-review and editing, Funding acquisition. Y. Huang: Conceptualization, Resources, Data curation, Writing-review and editing, Supervision; Project administration, Funding acquisition.

Data availability

Lake E5 core chronology, leaf wax hydrogen isotope data, and climate reconstructions, as well as the precipitation isotope data from the Toolik Field Station, are freely available at the Arctic Data Center Archives and at the NOAA National Centers for Environmental Information: https://www.ncdc.noaa.gov/paleo/study/33893.

Appendix A. Supplementary data

Supplementary data to this article can be found online at https://doi.org/10.1016/j.quascirev.2021.107130.

References

Abbott, M.B., Edwards, M.E., Finney, B.P., 2010. A 40,000-yr record of environmental change from Burial Lake in Northwest Alaska. Quat. Res. (Tokyo) 74, 156–165.
Abbott, M.B., Finney, B.P., Edwards, M.E., Kelts, K.R., 2000. Lake-level reconstruction and paleohydrology of Birch Lake, central Alaska, based on seismic reflection profiles and core transects. Quat. Res. (Tokyo) 53, 154–166.
Abbott, M.B., Stafford Jr., T.W., 1996. Radiocarbon geochemistry of modern and ancient arctic lake systems, baffin island, Canada. Quat. Res. (Tokyo) 45, 300–311.
Andersen, K.K., Azuma, N., Barnola, J.-M., Bigler, M., Biscaye, P., Caillon, N., Chappellaz, J., Clausen, H.B., Dahl-Jensen, D., Fischer, H., 2004. High-resolution record of Northern Hemisphere climate extending into the last interglacial period. Nature 431, 147–151.
Anderson, L., Abbott, M.B., Finney, B.P., 2001. Holocene climate inferred from oxygen isotope ratios in lake sediments, central Brooks Range, Alaska. Quat. Res. (Tokyo) 55, 313–321.
Andersson, R.A., Kuhry, P., Meyers, P., Zebühr, Y., Crill, P., Mörth, M., 2011. Impacts of paleohydrological changes on n-alkane biomarker compositions of a Holocene peat sequence in the eastern European Russian Arctic. Org. Geochem. 42, 1065–1075.
Appleby, P., Nolan, P., Gifford, D., Godfrey, M., Oldfield, F., Anderson, N., Battarbee, R., 1986. 210Pb dating by low background gamma counting. Hydrobiologia 143, 21–27.
Appleby, P., Oldfield, F., 1978. The calculation of lead-210 dates assuming a constant rate of supply of unsupported 210Pb to the sediment. Catena 5, 1–8.
Atkinson, T.C., Briffa, K.R., Coope, G., 1987. Seasonal temperatures in Britain during the past 22,000 years, reconstructed using beetle remains. Nature 325, 587–592.
Badding, M.E., Briner, J.P., Kaufman, D.S., 2013. 10Be ages of late Pleistocene deglaciation and Neoglaciation in the north-central Brooks Range, Arctic Alaska. J. Quat. Sci. 28, 95–102.
Bailey, H.L., Klein, E.S., Welker, J.M., 2019. Synoptic and mesoscale mechanisms drive winter precipitation δ18O/δ2H in south-central Alaska. J. Geophys. Res.: Atmosphere 124, 4252–4266.
Bartlein, P., Edwards, M., Hostetler, S., Shafer, S., Anderson, P., Brubaker, L., Lozhkin, A., 2015. Early-Holocene warming in Beringia and its mediation by sea-level and vegetation changes. Clim. Past Discuss 11, 873–932.
Bartlein, P., Harrison, S., Brewer, S., Connor, S., Davis, B., Gajewski, K., Guiot, J., Harrison-Prentice, T., Henderson, A., Peyron, O., 2011. Pollen-based continental climate reconstructions at 6 and 21 ka: a global synthesis. Clim. Dynam. 37, 775–802.
Berke, M.A., Sierra, A.C., Bush, R., Cheah, D., O'Connor, K., 2019. Controls on leaf wax fractionation and δ2H values in tundra vascular plants from western Greenland. Geochem. Cosmochim. Acta 244, 565–583.
Binford, M.W., 1990. Calculation and uncertainty analysis of 210Pb dates for PIRLA project lake sediment cores. J. Paleolimnol. 3, 253–267.
Blaauw, M., 2010. Methods and code for 'classical'age-modelling of radiocarbon sequences. Quat. Geochronol. 5, 512–518.
Bray, E., Evans, E., 1961. Distribution of n-paraffins as a clue to recognition of source beds. Geochem. Cosmochim. Acta 22, 2–15.
Briner, J.P., Kaufman, D.S., 2008. Late Pleistocene mountain glaciation in Alaska: key chronologies. J. Quat. Sci. 23, 659–670.
Broadman, E., Kaufman, D.S., Henderson, A.C., Malmierca-Vallet, I., Leng, M.J., Lacey, J.H., 2020. Coupled impacts of sea ice variability and North Pacific atmospheric circulation on Holocene hydroclimate in Arctic Alaska. Proc. Natl. Acad. Sci. Unit. States Am. 117, 33034–33042.
Broccoli, A.J., Manabe, S., 1987. The effects of the Laurentide ice sheet on North American climate during the last glacial maximum. Géogr. Phys. Quaternaire 41, 9.
Broecker, W.S., Kennett, J.P., Flower, B.P., Teller, J.T., Trumbore, S., Bonani, G., Wolfli, W., 1989. Routing of Meltwater from the Laurentide Ice Sheet during the Younger Dryas Cold Episode.
Buchwal, A., Sullivan, P.F., Macias-Fauria, M., Post, E., Myers-Smith, I.H., Stroeve, J.C., Blok, D., Tape, K.D., Forbes, B.C., Ropars, P., 2020. Divergence of Arctic shrub growth associated with sea ice decline. Proc. Natl. Acad. Sci. Unit. States Am. 117, 33334–33344.
Buizert, C., Gkinis, V., Severinghaus, J.P., He, F., Lecavalier, B.S., Kindler, P., Leuenberger, M., Carlson, A.E., Vinther, B., Masson-Delmotte, V., 2014. Greenland temperature response to climate forcing during the last deglaciation. Science 345, 1177–1180.
Cherry, J.E., Déry, S.J., Stieglitz, M., Pan, F.-f., 2014. Meteorology and climate of Toolik Lake and the north slope of Alaska: past, present and future. In: Alaska's Changing Arctic: Ecological Consequences for Tundra, Streams, and Lakes. Oxford Univ. Press.
Chikaraishi, Y., Naraoka, H., 2007. δ 13 C and δD relationships among three n-alkyl compound classes (n-alkanoic acid, n-alkane and n-alkanol) of terrestrial higher plants. Org. Geochem. 38, 198–215.
Chipman, M.L., Kling, G.W., Lundstrom, C.C., Hu, F.S., 2016. Multiple thermo-erosional episodes during the past six millennia: implications for the response of Arctic permafrost to climate change. Geology G37693, 37691.
Clark, J., Mitrovica, J.X., Alder, J., 2014. Coastal paleogeography of the California–Oregon–Washington and Bering Sea continental shelves during the latest Pleistocene and Holocene: implications for the archaeological record. J. Archaeol. Sci. 52, 12–23.
Crump, S.E., Miller, G.H., Power, M., Sepúlveda, J., Dildar, N., Coghlan, M., Bunce, M., 2019. Arctic shrub colonization lagged peak postglacial warmth: molecular evidence in lake sediment from Arctic Canada. Global Change Biol. 25, 4244–4256.
Dahl-Jensen, D., Mosegaard, K., Gundestrup, N., Clow, G.D., Johnsen, S.J., Hansen, A.W., Balling, N., 1998. Past temperatures directly from the Greenland ice sheet. Science 282, 268–271.
Daniels, W.C., Huang, Y., Russell, J.M., Giblin, A.E., 2018. Effect of continuous light on leaf wax isotope ratios in Betula nana and Eriophorum vaginatum: implications for Arctic paleoclimate reconstructions. Org. Geochem. 125, 70–81.
Daniels, W.C., Kling, G.W., Giblin, A.E., 2015. Benthic community metabolism in deep and shallow Arctic lakes during 13 years of whole–lake fertilization. Limnol. Oceanogr. (n/a-n/a).
Daniels, W.C., Russell, J.M., Giblin, A.E., Welker, J.M., Klein, E.S., Huang, Y., 2017. Hydrogen isotope fractionation in leaf waxes in the Alaskan Arctic tundra. Geochem. Cosmochim. Acta 213, 216–236.
Dansgaard, W., 1964. Stable isotopes in precipitation. Tellus 16, 436–468.
Denton, G., Alley, R., Comer, G., Broecker, W., 2005. The role of seasonality in abrupt climate change. Quat. Sci. Rev. 24, 1159–1182.
Dion-Kirschner, H., McFarlin, J.M., Masterson, A.L., Axford, Y., Osburn, M.R., 2020. Modern constraints on the sources and climate signals recorded by sedimentary plant waxes in west Greenland. Geochem. Cosmochim. Acta.
Dyke, A.S., 2004. An outline of North American deglaciation with emphasis on central and northern Canada. Quaternary glaciations: Extent and chronology 2, 373–424.
Eisner, W.R., Colinvaux, P.A., 1992. Late quaternary pollen records from Oil Lake and feniak lake, Alaska. U.S.A. Arct. Alp. Res. 24, 56–63.
Elder, C.D., Xu, X., Walker, J., Schnell, J.L., Hinkel, K.M., Townsend-Small, A., Arp, C.D., Pohlman, J.W., Gaglioti, B.V., Czimczik, C.I., 2018. Greenhouse gas emissions

from diverse Arctic Alaskan lakes are dominated by young carbon. Nat. Clim. Change 8, 166.
Elias, S.A., Short, S.K., Nelson, C.H., Birks, H.H., 1996. Life and times of the Bering land bridge. Nature 382, 60–63.
Elmendorf, S.C., Henry, G.H., Hollister, R.D., Björk, R.G., Boulanger-Lapointe, N., Cooper, E.J., Cornelissen, J.H., Day, T.A., Dorrepaal, E., Elumeeva, T.G., 2012. Plot-scale evidence of tundra vegetation change and links to recent summer warming. Nat. Clim. Change 2, 453.
England, J.H., Furze, M.F., 2008. New evidence from the western Canadian arctic archipelago for the resubmergence of Bering Strait. Quat. Res. (Tokyo) 70, 60–67.
Engstrom, D., Hansen, B., Wright, H., 1990. A possible Younger Dryas record in southeastern Alaska. Science 250, 1383–1385.
Epstein, S., 1995. The isotopic climatic records in the Alleröd-Bølling-Younger Dryas and Post-Younger Dryas events. Global Biogeochem. Cycles 9, 557–563.
Feakins, S.J., 2013. Pollen-corrected leaf wax D/H reconstructions of northeast African hydrological changes during the late Miocene. Palaeogeogr. Palaeoclimatol. Palaeoecol. 374, 62–71.
Baglioni, B.V., Mann, D.H., Wooller, M.J., Jones, B.M., Wiles, G.C., Groves, P., Kunz, M.L., Baughman, C.A., Reanier, R.E., 2017. Younger-Dryas cooling and sea-ice feedbacks were prominent features of the Pleistocene-Holocene transition in Arctic Alaska. Quat. Sci. Rev. 169, 330–343.
Gao, L., Edwards, E.J., Zeng, Y., Huang, Y., 2014. Major evolutionary trends in hydrogen isotope fractionation of vascular plant leaf waxes. PLoS One 9, e112610.
Goebel, T., Waters, M.R., O'rourke, D.H., 2008. The late Pleistocene dispersal of modern humans in the Americas. Science 319, 1497–1502.
Graf, K.E., Bigelow, N.H., 2011. Human response to climate during the Younger Dryas chronozone in central Alaska. Quat. Int. 242, 434–451.
Grootes, P., Stuiver, M., 1997. Oxygen 18/16 variability in Greenland snow and ice with 10− 3-to 105-year time resolution. J. Geophys. Res.: Oceans 102 (1978–2012), 26455–26470.
Grootes, P., Stuiver, M., White, J., Johnson, S., Jouzel, J., 1993. Comparison of oxygen isotope records from the GISP2 and GRIP Greenland ice cores. Nature 366, 3.
Hamilton, T.D., 2003. Glacial geology of the Toolik Lake and upper kuparuk river regions. In: Walker, D. (Ed.), Biological Papers of the University of Alaska. Institute of Arctic Biology, Fairbanks, Alaska.
Holland, K.M., Porter, T.J., Froese, D.G., Kokelj, S.V., Buchanan, C.A., 2020. Ice-wedge evidence of Holocene winter warming in the Canadian arctic. Geophys. Res. Lett. 47, e2020GL087942.
Hu, A., Meehl, G.A., Han, W., Abe-Ouchi, A., Morrill, C., Okazaki, Y., Chikamoto, M.O., 2012. The pacific-atlantic seesaw and the Bering Strait. Geophys. Res. Lett. 39.
Hu, A., Meehl, G.A., Han, W., Otto-Bliestner, B., Abe-Ouchi, A., Rosenbloom, N., 2015. Effects of the Bering Strait closure on AMOC and global climate under different background climates. Prog. Oceanogr. 132, 174–196.
Hu, F.S., Nelson, D.M., Clarke, G.H., Rühland, K.M., Huang, Y., Kaufman, D.S., Smol, J.P., 2006. Abrupt climatic events during the last glacial-interglacial transition in Alaska. Geophys. Res. Lett. 33.
Irvine, F., Cwynar, L.C., Vermaire, J.C., Rees, A.B., 2012. Midge-inferred temperature reconstructions and vegetation change over the last~ 15,000 years from Trout Lake, northern Yukon Territory, eastern Beringia. J. Paleolimnol. 48, 133–146.
Jakobsson, M., Pearce, C., Cronin, T.M., Backman, J., Anderson, L.G., Barrientos, N., Björk, G., Coxall, H., De Boer, A., Mayer, L.A., 2017. Post-glacial flooding of the Bering Land Bridge dated to 11 cal ka BP based on new geophysical and sediment records. Clim. Past 13, 991.
Jespersen, R.G., Leffler, A.J., Oberbauer, S.F., Welker, J.M., 2018. Arctic plant ecophysiology and water source utilization in response to altered snow: isotopic (δ 18 O and δ 2 H) evidence for meltwater subsidies to deciduous shrubs. Oecologia 187, 1009–1023.
Johnsen, S.J., Clausen, H.B., Dansgaard, W., Fuhrer, K., Gundestrup, N., Hammer, C.U., Iversen, P., Jouzel, J., Stauffer, B., Steffensen, J.P., 1992. Irregular glacial interstadials recorded in a new Greenland ice core. Nature 359, 3.
Jones, M.C., Berkelhammer, M., Keller, K.J., Yoshimura, K., Wooller, M.J., 2020. High sensitivity of Bering Sea winter sea ice to winter insolation and carbon dioxide over the last 5500 years. Science advances 6, eaaz9588.
Jones, M.C., Yu, Z., 2010. Rapid deglacial and early Holocene expansion of peatlands in Alaska. Proc. Natl. Acad. Sci. Unit. States Am. 107, 7347–7352.
Jones, P.D., Lister, D.H., Osborn, T.J., Harpham, C., Salmon, M., Morice, C.P., 2012. Hemispheric and large-scale land-surface air temperature variations: an extensive revision and an update to 2010. J. Geophys. Res.: Atmosphere 117 (n/a-n/a).
Kaufman, D., 2004. Holocene thermal maximum in the western Arctic (0–180°W). Quat. Sci. Rev. 23, 529–560.
Kaufman, D.S., Schneider, D.P., McKay, N.P., Ammann, C.M., Bradley, R.S., Briffa, K.R., Miller, G.H., Otto-Bliesner, B.L., Overpeck, J.T., Vinther, B.M., 2009. Recent warming reverses long-term arctic cooling. Science 325, 1236–1239.
Keigwin, L.D., Donnelly, J.P., Cook, M.S., Driscoll, N.W., Brigham-Grette, J., 2006. Rapid sea-level rise and Holocene climate in the Chukchi Sea. Geology 34, 861–864.
Keisling, B.A., Castañeda, I.S., Brigham-Grette, J., 2017. Hydrological and temperature change in arctic siberia during the intensification of northern hemisphere glaciation. Earth Planet Sci. Lett. 457, 136–148.
Kienast, S.S., McKay, J.L., 2001. Sea surface temperatures in the subarctic northeast Pacific reflect millennial-scale climate oscillations during the last 16 kyrs. Geophys. Res. Lett. 28, 1563–1566.
Klein, E.S., Nolan, M., McConnell, J., Sigl, M., Cherry, J., Young, J., Welker, J.M., 2015. McCall Glacier record of Arctic climate change: interpreting a northern Alaska ice core with regional water isotopes. Quat. Sci. Rev.
Köhler, P., Nehrbass-Ahles, C., Schmitt, J., Stocker, T.F., Fischer, H., 2017. A 156 kyr smoothed history of the atmospheric greenhouse gases CO2, CH4, and N2O and their radiative forcing. Earth Syst. Sci. Data 9, 363–387.
Kokorowski, H., Anderson, P., Mock, C., Lozhkin, A., 2008. A re-evaluation and spatial analysis of evidence for a Younger Dryas climatic reversal in Beringia. Quat. Sci. Rev. 27, 1710–1722.
Konecky, B., Russell, J., Bijaksana, S., 2016. Glacial aridity in central Indonesia coeval with intensified monsoon circulation. Earth Planet Sci. Lett. 437, 15–24.
Kühn, H., Lembke-Jene, L., Gersonde, R., Esper, O., Lamy, F., Arz, H., Kuhn, G., Tiedemann, R., 2014. Laminated sediments in the Bering Sea reveal atmospheric teleconnections to Greenland climate on millennial to decadal timescales during the last deglaciation. Clim. Past 10, 2215–2236.
Kurek, J., Cwynar, L.C., Ager, T.A., Abbott, M.B., Edwards, M.E., 2009a. Late Quaternary paleoclimate of western Alaska inferred from fossil chironomids and its relation to vegetation histories. Quat. Sci. Rev. 28, 799–811.
Kurek, J., Cwynar, L.C., Vermaire, J.C., 2009b. A late quaternary paleotemperature record from Hanging Lake, northern Yukon territory, eastern Beringia. Quat. Res. (Tokyo) 72, 246–257.
Lachniet, M.S., Lawson, D.E., Stephen, H., Sloat, A.R., Patterson, W.P., 2016. Isoscapes of δ18O and δ2H reveal climatic forcings on Alaska and Yukon precipitation. Water Resour. Res. 52, 6575–6586.
Ladd, S.N., Maloney, A.E., Nelson, D.B., Prebble, M., Camperio, G., Sear, D.A., Hassall, J.D., Langdon, P.G., Sachs, J.P., Dubois, N., 2021. Leaf wax hydrogen isotopes as a hydroclimate proxy in the tropical pacific. J. Geophys. Res.: Biogeosciences 126, e2020JG005891.
Laskar, J., Robutel, P., Joutel, F., Gastineau, M., Correia, A., Levrard, B., 2004. A long-term numerical solution for the insolation quantities of the Earth. Astron. Astrophys. 428, 261–285.
Li, C., Battisti, D.S., Schrag, D.P., Tziperman, E., 2005. Abrupt climate shifts in Greenland due to displacements of the sea ice edge. Geophys. Res. Lett. 32.
Lisiecki, L.E., Raymo, M.E., 2005. A Pliocene-Pleistocene stack of 57 globally distributed benthic δ18O records. Paleoceanography 20.
Liu, Z., Otto-Bliesner, B., He, F., Brady, E., Tomas, R., Clark, P., Carlson, A., Lynch-Stieglitz, J., Curry, W., Brook, E., 2009. Transient simulation of last deglaciation with a new mechanism for Bølling-Allerød warming. Science 325, 310–314.
Liu, Z., Wen, X., Brady, E., Otto-Bliesner, B., Yu, G., Lu, H., Cheng, H., Wang, Y., Zheng, W., Ding, Y., 2014. Chinese cave records and the East Asia summer monsoon. Quat. Sci. Rev. 83, 115–128.
Livingstone, D., 1955. Some pollen profiles from arctic Alaska. Ecology 587–600.
Löfverström, M., Liakka, J., 2016. On the limited ice intrusion in Alaska at the LGM. Geophys. Res. Lett. 43 (11), 030-011,038.
Longo, W.M., Huang, Y., Russell, J.M., Morrill, C., Daniels, W.C., Giblin, A.E., Crowther, J., 2020. Insolation and greenhouse gases drove Holocene winter and spring warming in Arctic Alaska. Quat. Sci. Rev. 242, 106438.
Longo, W.M., Theroux, S., Giblin, A.E., Zheng, Y., Dillon, J.T., Huang, Y., 2016. Temperature calibration and phylogenetically distinct distributions for freshwater alkenones: evidence from northern Alaskan lakes. Geochem. Cosmochim. Acta 180, 177–196.
Lynch, A., Chapin III, F., Hinzman, L., Wu, W., Lilly, E., Vourlitis, G., Kim, E., 1999. Surface energy balance on the arctic tundra: measurements and models. J. Clim. 12.
Maier, E., Zhang, X., Abelmann, A., Gersonde, R., Mulitza, S., Werner, M., Méheust, M., Ren, J., Chapligin, B., Meyer, H., Stein, R., Tiedemann, R., Lohmann, G., 2018. North Pacific freshwater events linked to changes in glacial ocean circulation. Nature 559, 241–245.
Mangerud, J., Briner, J.P., Goslar, T., Svendsen, J.I., 2017. The Bølling-age Blomvåg Beds, western Norway: implications for the Older Dryas glacial re-advance and the age of the deglaciation. Boreas 46, 162–184.
Manley, W.F., Kaufman, D., 2002. Alaska Paleoglacier Atlas. Institute of Arctic and Alpine Research (INSTAAR), University of Colorado, Boulder, CO.
Mann, D.H., Groves, P., Kunz, M.L., Reanier, R.E., Gaglioti, B.V., 2013. Ice-age megafauna in Arctic Alaska: extinction, invasion, survival. Quat. Sci. Rev. 70, 91–108.
Mann, D.H., Groves, P., Reanier, R.E., Kunz, M.L., 2010. Floodplains, permafrost, cottonwood trees, and peat: what happened the last time climate warmed suddenly in arctic Alaska? Quat. Sci. Rev. 29, 3812–3830.
Mann, D.H., Peteet, D.M., Reanier, R.E., Kunz, M.L., 2002. Responses of an arctic landscape to Lateglacial and early Holocene climatic changes: the importance of moisture. Quat. Sci. Rev. 21, 997–1021.
Mann, D.H., Reanier, R.E., Peteet, D.M., Kunz, M.L., Johnson, M., 2001. Environmental change and arctic paleoindians. Arctic Anthropol. 119–138.
McFarlin, J.M., Axford, Y., Masterson, A.L., Osburn, M.R., 2019. Calibration of modern sedimentary δ2H plant wax-water relationships in Greenland lakes. Quat. Sci. Rev. 225, 105978.
McManus, J.F., Francois, R., Gherardi, J.M., Keigwin, L.D., Brown-Leger, S., 2004. Collapse and rapid resumption of Atlantic meridional circulation linked to deglacial climate changes. Nature (London) 428, 834.
Mellat, M., Mustonen, K.-R., Bailey, H.L., Klein, E.S., Marttila, H., Welker, J.M., Submitted. Pan-Arctic summer moisture sources revealed using an event-based precipitation isotope (δ18O, δ2H, d-excess) network (PAPIN. Earth. Planet. Sci. Lett.
Melles, M., Brigham-Grette, J., Minyuk, P.S., Nowaczyk, N.R., Wennrich, V., DeConto, R.M., Anderson, P.M., Andreev, A.A., Coletti, A., Cook, T.L., Haltia-

Hovi, E., Kukkonen, M., Lozhkin, A.V., Rosén, P., Tarasov, P., Vogel, H., Wagner, B., 2012. 2.8 million years of arctic climate change from Lake El'gygytgyn, NE Russia. Science 337, 315–320.
Meyer, H., Schirrmeister, L., Yoshikawa, K., Opel, T., Wetterich, S., Hubberten, H.W., Brown, J., 2010. Permafrost evidence for severe winter cooling during the Younger Dryas in northern Alaska. Geophys. Res. Lett. 37.
Miller, G.H., Alley, R.B., Brigham-Grette, J., Fitzpatrick, J.J., Polyak, L., Serreze, M.C., White, J.W.C., 2010. Arctic amplification: can the past constrain the future? Quat. Sci. Rev. 29, 1779–1790.
Nichols, J.E., Peteet, D.M., Moy, C.M., Castañeda, I.S., McGeachy, A., Perez, M., 2014. Impacts of climate and vegetation change on carbon accumulation in a south-central Alaskan peatland assessed with novel organic geochemical techniques. Holocene 24, 1146–1155.
O'Connor, K.F., Berke, M.A., Ziolkowski, L.A., 2020. Hydrogen isotope fractionation in modern plants along a boreal-tundra transect in Alaska. Org. Geochem. 147, 104064.
Okazaki, Y., Timmermann, A., Menviel, L., Harada, N., Abe-Ouchi, A., Chikamoto, M., Mouchet, A., Asahi, H., 2010. Deepwater formation in the North Pacific during the last glacial termination. Science 329, 200–204.
Oswald, W.W., Anderson, P.M., Brown, T.A., Brubaker, L.B., Hu, F.S., Lozhkin, A.V., Tinner, W., Kaltenrieder, P., 2005. Effects of sample mass and macrofossil type on radiocarbon dating of arctic and boreal lake sediments. Holocene 15, 758–767.
Oswald, W.W., Brubaker, L.B., Anderson, P.M., 1999. Late Quaternary vegetational history of the Howard Pass area, northwestern Alaska. Can. J. Bot. 77, 570–581.
Otto-Bliesner, B.L., Brady, E.C., Clauzet, G., Tomas, R., Levis, S., Kothavala, Z., 2006. Last glacial maximum and Holocene climate in CCSM3. J. Clim. 19, 2526–2544.
Pautler, B.G., Reichart, G.-J., Sanborn, P.T., Simpson, M.J., Weijers, J.W., 2014. Comparison of soil derived tetraether membrane lipid distributions and plant-wax δD compositions for reconstruction of Canadian Arctic temperatures. Palaeogeogr. Palaeoclimatol. Palaeoecol. 404, 78–88.
Pendleton, S.L., Ceperley, E.G., Briner, J.P., Kaufman, D.S., Zimmerman, S., 2015. Rapid and early deglaciation in the central Brooks Range. Arctic Alaska. Geology 43, 419–422.
Pico, T., Mitrovica, J., Mix, A., 2020. Sea level fingerprinting of the Bering Strait flooding history detects the source of the Younger Dryas climate event. Science advances 6, eaay2935.
Porter, T.J., Froese, D.G., Feakins, S.J., Bindeman, I.N., Mahony, M.E., Pautler, B.G., Reichart, G.-J., Sanborn, P.T., Simpson, M.J., Weijers, J.W.H., 2016. Multiple water isotope proxy reconstruction of extremely low last glacial temperatures in Eastern Beringia (Western Arctic). Quat. Sci. Rev. 137, 113–125.
Porter, T.J., Schoenemann, S.W., Davies, L.J., Steig, E.J., Bandara, S., Froese, D.G., 2019. Recent summer warming in northwestern Canada exceeds the Holocene thermal maximum. Nat. Commun. 10, 1631.
Praetorius, S.K., Mix, A.C., 2014. Synchronization of North Pacific and Greenland climates preceded abrupt deglacial warming. Science 345, 444–448.
Putman, A.L., Feng, X., Sonder, L.J., Posmentier, E.S., 2017. Annual variation in event-scale precipitation δ 2 H at Barrow, AK, reflects vapor source region. Atmos. Chem. Phys. 17, 4627–4639.
Rae, J.W., Gray, W., Wills, R., Eisenman, I., Fitzhugh, B., Fotheringham, M., Littley, E., Rafter, P., Rees-Owen, R., Ridgwell, A., 2020. Overturning circulation, nutrient limitation, and warming in the Glacial North Pacific. Science advances 6, eabd1654.
Reimer, P.J., Bard, E., Bayliss, A., Beck, J.W., Blackwell, P.G., Bronk Ramsey, C., Buck, C.E., Cheng, H., Edwards, R.L., Friedrich, M., 2013. IntCal13 and Marine13 Radiocarbon Age Calibration Curves 0-50,000 Years Cal BP.
Sachse, D., Billault, I., Bowen, G.J., Chikaraishi, Y., Dawson, T.E., Feakins, S.J., Freeman, K.H., Magill, C.R., McInerney, F.A., Van der Meer, M.T., 2012. Molecular paleohydrology: interpreting the hydrogen-isotopic composition of lipid biomarkers from photosynthesizing organisms. Annu. Rev. Earth Planet Sci. 40, 221–249.
Sarnthein, M., Kiefer, T., Grootes, P.M., Elderfield, H., Erlenkeuser, H., 2006. Warmings in the far northwestern Pacific promoted pre-Clovis immigration to America during Heinrich event 1. Geology 34, 141–144.
Schmidt, G.A., Bigg, G.R., Rohling, E.J., 1999. In: Global Seawater Oxygen-18 Database - V1, p. 21.
Schrag, D.P., Hampt, G., Murray, D.W., 1996. Pore fluid constraints on the temperature and oxygen isotopic composition of the glacial ocean. Science 272, 1930.
Serreze, M.C., Holland, M.M., Stroeve, J., 2007. Perspectives on the Arctic's shrinking sea-ice cover. Science 315, 1533–1536.
Severinghaus, J.P., Brook, E.J., 1999. Abrupt climate change at the end of the last glacial period inferred from trapped air in polar ice. Science 286, 930–934.
Shah Walter, S.R., Gagnon, A.R., Roberts, M.L., McNichol, A.P., Gaylord, M.C.L., Klein, E., 2015. Ultra-small graphitization reactors for ultra-microscale 14 C analysis at the National Ocean Sciences accelerator mass spectrometry (NOSAMS) facility. Radiocarbon 57, 109–122.
Shakun, J.D., Carlson, A.E., 2010. A global perspective on Last Glacial Maximum to Holocene climate change. Quat. Sci. Rev. 29, 1801–1816.
Stabeno, P.J., Schumacher, J.D., Ohtani, K., 1999. The physical oceanography of the Bering Sea: a summary of physical, chemical, and biological characteristics, and a synopsis of research on the Bering Sea. In: Laughlin, T.R., Ohtani, K. (Eds.), Dynamics of the Bering Sea. TR Loughlin and K. Ohtani. North Pacific Marine Science Organization.
Stroeve, J.C., Kattsov, V., Barrett, A., Serreze, M., Pavlova, T., Holland, M., Meier, W.N., 2012. Trends in Arctic sea ice extent from CMIP5, CMIP3 and observations. Geophys. Res. Lett. 39.
Sturm, M., Racine, C., Tape, K., 2001. Climate change: increasing shrub abundance in the Arctic. Nature 411, 546–547.
Tharammal, T., Paul, A., Merkel, U., Noone, D., 2013. Influence of Last Glacial Maximum boundary conditions on the global water isotope distribution in an atmospheric general circulation model. Clim. Past 9, 789.
Thomas, E.K., Clemens, S.C., Prell, W.L., Herbert, T.D., Huang, Y., Liu, Z., Sinninghe Damsté, J.S., Sun, Y., Wen, X., 2014. Temperature and leaf wax δ2H records demonstrate seasonal and regional controls on Asian monsoon proxies. Geology 42, 1075–1078.
Thomas, E.K., McGrane, S., Briner, J.P., Huang, Y., 2012. Leaf wax δ 2 H and varve-thickness climate proxies from proglacial lake sediments, Baffin Island, Arctic Canada. J. Paleolimnol. 1–15.
Tierney, J.E., Zhu, J., King, J., Malevich, S.B., Hakim, G.J., Poulsen, C.J., 2020. Glacial cooling and climate sensitivity revisited. Nature 584, 569–573.
Toolik Environmental Data Center Team, 2016. Meteorological Monitoring Program at Toolik, Alaska. Toolik Field Station, Institute of Arctic Biology, University of Alaska Fairbanks.
Toolik, G.I.S., 2019. In: Sensing, T.F.S.G.a.R. (Ed.), Toolik Field Station Bathymetry.
Vachula, R.S., Chipman, M.L., Hu, F.S., 2017. Holocene climatic change in the Alaskan Arctic as inferred from oxygen-isotope and lake-sediment analyses at Wahoo Lake. Holocene.
Vachula, R.S., Huang, Y., Longo, W.M., Dee, S.G., Daniels, W.C., Russell, J.M., 2019. Evidence of Ice Age humans in eastern Beringia suggests early migration to North America. Quat. Sci. Rev. 205, 35–44.
Viau, A., Gajewski, K., Sawada, M., Bunbury, J., 2008. Low-and high-frequency climate variability in eastern Beringia during the past 25 000 years. Can. J. Earth Sci. 45, 1435–1453.
Welker, J., 2000. Isotopic (δ18O) characteristics of weekly precipitation collected across the USA: an initial analysis with application to water source studies. Hydrol. Process. 14, 1449–1464.
Welker, J.M., 2012. ENSO effects on δ18O, δ2H and d-excess values in precipitation across the US using a high-density, long-term network (USNIP). Rapid Commun. Mass Spectrom. 26, 1893–1898.
Welker, J.M., Rayback, S., Henry, G.H., 2005. Arctic and North Atlantic Oscillation phase changes are recorded in the isotopes (δ18O and δ13C) of Cassiope tetragona plants. Global Change Biol. 11, 997–1002.
Wetterich, S., Rudaya, N., Tumskoy, V., Andreev, A.A., Opel, T., Schirrmeister, L., Meyer, H., 2011. Last glacial maximum records in permafrost of the east siberian arctic. Quat. Sci. Rev. 30, 3139–3151.
Wilkie, K., Chapligin, B., Meyer, H., Burns, S., Petsch, S., Brigham-Grette, J., 2012. Modern isotope hydrology and controls on δD of plant leaf waxes at Lake El'gygytgyn, NE Russia. Clim. Past Discuss 8, 3719–3764.
Wooller, M.J., Pohlman, J.W., Gaglioti, B.V., Langdon, P., Jones, M., Anthony, K.M.W., Becker, K.W., Hinrichs, K.-U., Elvert, M., 2012. Reconstruction of past methane availability in an Arctic Alaska wetland indicates climate influenced methane release during the past~ 12,000 years. J. Paleolimnol. 48, 27–42.
Yang, H., Huang, Y., 2003. Preservation of lipid hydrogen isotope ratios in Miocene lacustrine sediments and plant fossils at Clarkia, northern Idaho, USA. Org. Geochem. 34, 413–423.
Young, N.E., Briner, J.P., Schaefer, J., Zimmerman, S., Finkel, R.C., 2019. Early Younger Dryas glacier culmination in southern Alaska: implications for North Atlantic climate change during the last deglaciation. Geology 47, 550–554.
Zimov, S., Zimov, N., Tikhonov, A., Chapin, F., 2012. Mammoth steppe: a high-productivity phenomenon. Quat. Sci. Rev. 57, 26–45.